



RESEARCH

The *Fusarium graminearum* Effector Protease FgTPP1 Suppresses Immune Responses and Facilitates Fusarium Head Blight Disease

Martin Darino,¹ Namrata Jaiswal,² Reynaldi Darma,¹ Erika Kroll,¹  Martin Urban,¹ Youhuang Xiang,³ Moumita Srivastava,¹ Hye-Seon Kim,⁴ Ariana Myers,² Steven R. Scofield,² Roger W. Innes,³  Kim E. Hammond-Kosack,^{1,†} and Matthew Helm^{2,†}

¹ Protecting Crops and the Environment, Rothamsted Research, Harpenden, Hertfordshire, AL5 2JQ, U.K.

² Crop Production and Pest Control Research Unit, U.S. Department of Agriculture-Agricultural Research Service (USDA-ARS), West Lafayette, IN 47907, U.S.A.

³ Department of Biology, Indiana University, Bloomington, IN 47405, U.S.A.

⁴ National Center for Agricultural Utilization Research, Mycotoxin Prevention and Applied Microbiology Research Unit, U.S. Department of Agriculture-Agricultural Research Service (USDA-ARS), Peoria, IL 61604, U.S.A.

Accepted for publication 22 January 2025.

Most plant pathogens secrete effector proteins to circumvent host immune responses, thereby promoting pathogen virulence. One such pathogen is the fungus *Fusarium graminearum*, which causes Fusarium head blight (FHB) disease on wheat and barley. Transcriptomic analyses revealed that *F. graminearum* expresses many candidate effector proteins during early phases

of the infection process, some of which are annotated as proteases. However, the contributions of these proteases to virulence remain poorly defined. Here, we characterize an *F. graminearum* endopeptidase, FgTPP1 (FGSG_11164), that is highly upregulated during wheat spikelet infection and is secreted from fungal cells. To elucidate the potential role of FgTPP1 in *F. graminearum* virulence, we generated *FgTPP1* deletion mutants ($\Delta Fgtp1$) and performed FHB infection assays. Deletion of *FgTPP1* reduced the virulence of *F. graminearum* as assessed by spikelet bleaching. Infection with wild-type *F. graminearum* induced full bleaching in about 50% of the spikes at 10 to 11 days postinfection, whereas this fraction was reduced to between 18 and 27% when using $\Delta Fgtp1$ mutants. Transient expression of green fluorescent protein-tagged FgTPP1 revealed that FgTPP1 localizes, in part, to chloroplasts and attenuates chitin-mediated activation of mitogen-activated protein kinase signaling, reactive oxygen species production, and cell death induced by an autoactive disease resistance protein when expressed in planta. Notably, the FgTPP1 protein is conserved across the Ascomycota phylum, suggesting that it may be a core effector among ascomycete plant pathogens. These properties make FgTPP1 an ideal candidate for decoy substrate engineering, with the goal of engineering resistance to FHB.

[†]Corresponding authors: M. Helm; Matthew.Helm@usda.gov, and K. E. Hammond-Kosack; kim.hammond-kosack@rothamsted.ac.uk

M. Darino, N. Jaiswal, and R. Darma contributed equally to this work.

Current address of M. Srivastava: Rajiv Gandhi Centre for Biotechnology, Thiruvananthapuram, Kerala, India.

Current address of A. Myers: Axbio Inc., Santa Clara, CA 95054, U.S.A.

All opinions expressed in this paper are the authors' and do not necessarily reflect the policies and views of USDA. Mention of trade names or commercial products in this publication is solely for the purpose of providing specific information and does not imply recommendation or endorsement by the U.S. Department of Agriculture. USDA is an equal opportunity provider and employer.

Funding: This research was supported by the United States Department of Agriculture-Agricultural Research Service (USDA-ARS) research project 5020-21220-014-00D, the U.S. Wheat and Barley Scab Initiative (award number 58-5020-0-013), and the USDA-National Institute of Food and Agriculture (NIFA) grant awarded to R. W. Innes and M. Helm (award number 2022-67013-38265). R. Darma is supported by a grant from the Biotechnology and Biological Sciences Research Council (BBSRC) (BB/X012131/1). Additional funding to support K. E. Hammond-Kosack, M. Urban, and M. Darino has been provided by the BBSRC Institute Strategic Programme (ISP) Grants Designing Future Wheat (BBS/E/C/00010250) and Delivering Sustainable Wheat (BB/X011003/1 and BBS/E/RH/230001B) and the BBSRC grant (BB/X012131/1). E. Kroll is supported by the BBSRC-funded South West Biosciences Doctoral Training Partnership (BB/T008741/1). The funding bodies had no role in designing the experiments, collecting the data, or writing the manuscript.

e-Xtra: Supplementary material is available online.

The author(s) declare no conflict of interest.

Keywords: cell death, chloroplast, *Fusarium graminearum*, Fusarium head blight disease, immune suppression, MAPK, pathogenesis, protease, ROS, wheat (*Triticum aestivum*)

Most fungal phytopathogens express and secrete a repertoire of proteins known as effectors during pathogenesis that modulate plant cell defense responses to facilitate infection and thus disease progression (Bentham et al. 2020). Once secreted, effectors can either be retained in the plant apoplast or translocated directly into host cells, where they target multiple host proteins, thereby interfering with host cell-derived defense responses (Selin et al. 2016). To circumvent the immune-modulating activities of effectors, plants have evolved a two-tiered immune signaling network composed primarily of cell surface-localized and intracellular immune receptors (Chen et al. 2022; McCombe et al. 2022; Rhodes et al. 2022). Activation of cell surface-localized



Copyright © 2025 The Author(s). This is an open access article distributed under the CC BY-NC-ND 4.0 International license.

immune receptors by pathogen-associated molecular patterns (PAMPs) initiates an intracellular immune signaling cascade that includes, in part, the increased production of extracellular reactive oxygen species (ROS), upregulation of defense-related gene expression, and activation of mitogen-activated protein kinase (MAPK) signaling (Chen et al. 2022; McCombe et al. 2022; Rhodes et al. 2022). In turn, fungal phytopathogens have evolved effectors that are capable of suppressing ROS generation and accumulation, as well as MAPK signaling (Bentham et al. 2020; Chen et al. 2022; Deng et al. 2022; Ngou et al. 2022; Rogers et al. 2024).

Translocated effectors secreted by phytopathogens are diverse in terms of their sizes and specific functions. In the case of bacterial phytopathogens, many effectors have been shown to function as proteases that target specific host proteins to inactivate them (Chandrasekaran et al. 2016; Jashni et al. 2015). For example, the AvrRpt2 protease from *Pseudomonas syringae* is secreted into *Arabidopsis* host cells, where it cleaves *Arabidopsis* RPM1-interacting protein 4 (RIN4) at two positions (Kim et al. 2005). RIN4 also interacts with proteins in the exocyst complex and appears to regulate callose deposition in response to AvrRpm1 (Kim et al. 2005; Redditt et al. 2019). Similarly, the cysteine protease AvrPphB from *P. syringae* pv. *phaseolicola* targets a family of serine/threonine receptor-like cytoplasmic kinases involved in regulating cell surface-mediated immunity, rendering these kinases inactive (Shao et al. 2003; Zhang et al. 2010). In *Arabidopsis*, cleavage of one of these kinases, PBS1, by AvrPphB activates the intracellular immune receptor, RPS5, which initiates a signal-transduction cascade culminating in resistance to *P. syringae* strains expressing AvrPphB (Ade et al. 2007; Shao et al. 2003; Simonich and Innes 1995). Importantly, investigating how the *Arabidopsis* PBS1-RPS5 immune signaling module is activated by the AvrPphB protease has enabled researchers to bioengineer new-to-nature disease resistance specificities against plant pathogens in *Arabidopsis* as well as crop plants (Carter et al. 2019; Helm et al. 2019; Kim et al. 2016; Pottinger et al. 2020).

The ascomycete fungal pathogen *Fusarium graminearum* causes Fusarium head blight (FHB) disease in wheat (*Triticum* species), barley (*Hordeum vulgare*), and other cereal crops, often causing premature senescence and blighting of wheat floral tissues (Armer et al. 2024a; Dean et al. 2012; Figueroa et al. 2018; Kanja et al. 2021). FHB is considered one of the most economically important fungal diseases of cereal grains, with estimated economic losses exceeding approximately US\$1 billion annually in direct and indirect effects (Figueroa et al. 2018; Njanje et al. 2004). In addition to reducing overall grain yields, FHB disease contaminates the remaining grain with sesquiterpenoid trichothecene mycotoxins such as deoxynivalenol (DON), which, in turn, affects grain marketability and threatens food safety (Figueroa et al. 2018; Hohn and Desjardins 1992; Johns et al. 2022). *F. graminearum* employs a hemibiotrophic infection strategy to colonize different host structures, such as wheat floral tissues and coleoptiles (Armer et al. 2024b; Brown et al. 2011; Mentges et al. 2020; Qiu et al. 2019). During the symptomless infection phase, unbranched hyphae spread on the exterior surfaces of the host and form appressoria-like infection cushion structures that enable direct penetration of the cell wall of wheat cells (Mentges et al. 2020; Qiu et al. 2019). Once established, the fungus develops bulbous biotrophic hyphae that branch and push into the host cell, displacing the central vacuole (Qiu et al. 2019). Importantly, the plasma membrane of the invaded wheat cells remains intact, indicating that the early phases of infection are biotrophic (Brown et al. 2017; Qiu et al. 2019). During the later combined asymptomatic and symptomatic phases of disease development, *F. graminearum* develops extracellular hyphae to advance within and colonize the apoplastic environ-

ment (Brown et al. 2011; Qiu et al. 2019). Coincident with the appearance of disease symptoms, hyphae penetrate into adjacent wheat cells, and this change is often accompanied by host cell death (Brown et al. 2011; Qiu et al. 2019). The DON mycotoxin is required for successful traversing of the plasmodesmatal connections between wheat cells (Armer et al. 2024b). Collectively, fungal internal colonization and systemic spread through the wheat rachis results in bleached spikelets (Brown et al. 2012, 2017).

Similar to other plant-pathogenic fungi, *F. graminearum* is predicted to secrete effector proteins during early phases of infection (Brown et al. 2012, 2017; Hao et al. 2020, 2023; Lu and Edwards 2016; Miltenburg et al. 2022). However, our general knowledge of how *F. graminearum* effector proteins contribute to plant pathogenesis remains limited. Nevertheless, several *F. graminearum* effectors have been identified and reported to have a functional role in fungal pathogenicity. For example, Jiang et al. (2020) showed that *F. graminearum* secretes an effector protein designated FgOSP24 (Orphan Secreted Protein 24) into the host cell cytoplasm, where it subsequently interacts with and promotes the degradation of the SNF1-related kinase TaSnRK1a. Recent work by Hao et al. (2023) identified an *F. graminearum* effector, FGSG_04563 (FgNls1), that is highly expressed during early phases of FHB disease development, localizes to plant cell nuclei, and interacts with wheat histone 2B (TaH2B). Importantly, deletion of *FgNls1* from *F. graminearum* reduces disease progression within wheat spikes. Host-induced silencing of *FgNls1* suppresses FHB disease development, indicating a functional role for FgNls1 in fungal pathogenesis (Hao et al. 2023). Similarly, two candidate *F. graminearum* effectors, ARB93B and FGSG_01831, have been shown to be expressed during the early stages of infection and to suppress cell surface-triggered immune responses, including PAMP-triggered ROS production (Hao et al. 2019, 2020).

In addition to the aforementioned *F. graminearum* effectors, two candidate effector proteases have been identified that appear to contribute to *F. graminearum* virulence. Specifically, deletion of genes encoding a fungalyisin metallopeptidase known as FgFly1 (FGSG_03467) and a subtilisin-like protease termed FgPrb1 (FGSG_00192) attenuates *F. graminearum* virulence and FHB disease progression in wheat spikes (Wang et al. 2022; Xu et al. 2020). Recent work by Xiong et al. (2024) identified five subtilisin-like proteases from *F. graminearum* (FgSLP1-5) that trigger cell death in *Nicotiana benthamiana*, *Arabidopsis*, and cotton (*Gossypium barbadense*). These cell death-inducing activities were independent of BAK1, SOBIR1, EDS1, and PAD4-mediated signaling. Importantly, *F. graminearum* mutants lacking two subtilisin-like proteases, FgSLP1 and FgSLP2, showed reduced fungal virulence in wheat, demonstrating that FgSLP1 and FgSLP2 likely contribute to virulence (Xiong et al. 2024). Recently, J. Liu et al. (2024) identified a serine carboxypeptidase, FgSCP (FGSG_08454), that is expressed during early FHB disease development. Deletion of FgSCP inhibits fungal reproduction, alters vegetative growth, and reduces *F. graminearum* virulence and DON biosynthesis in wheat (J. Liu et al. 2024). Collectively, these studies highlight the important roles of *F. graminearum* proteases during pathogenicity. However, despite the importance of *F. graminearum* globally, host proteins that are targeted by effector proteases from this fungus have yet to be identified.

To further understand how candidate secreted effector proteases from *F. graminearum* contribute to fungal virulence, we initially took a computational biology approach to identify the predicted secreted proteases present in the most recent *F. graminearum* genome annotation and identified one candidate protease, FGSG_11164 (FGRAMPH1_01G21371), that was highly expressed during floral wheat spike colonization (Brown et al.

2012, 2017; King et al. 2015, 2017a). FGSG_11164 encodes a putative trypsin precursor protein and, therefore, has been designated FgTPP1 (*F. graminearum* Trypsin precursor protein 1). Here, we show that the predicted signal peptide from FgTPP1 is functional and facilitates secretion of FgTPP1 from fungal cells. Importantly, *F. graminearum* mutants lacking FgTPP1 expression ($\Delta Fgtp1$) showed a significantly slower disease progression and colonization of wheat spikes when compared with the wild-type *F. graminearum* PH-1, indicating that FgTPP1 contributes to fungal virulence. *Agrobacterium*-mediated transient expression of green fluorescent protein (GFP)-tagged FgTPP1 in *N. benthamiana* leaves revealed that FgTPP1 localizes, in part, to chloroplast stroma and attenuates chitin-mediated activation of MAPK signaling, ROS production, and cell death induced by an autoactive disease resistance protein, demonstrating that FgTPP1 suppresses multiple plant immune responses. Lastly, we show that the TPP1 protein is conserved in fungal species from different genera of the Ascomycota phylum, suggesting a conserved role(s) for TPP1 in different plant-infecting fungi.

Results

F. graminearum strain PH-1 expresses multiple candidate effector proteases during early wheat spikelet infection

To identify putative effector proteases secreted by *F. graminearum*, we searched the most recent genome annotation of *F. graminearum* (YL1 version, NCBI GenBank number: PRJNA782099) for the terms “peptidase” and “protease” and screened this gene subset for the presence of signal peptides, which would suggest the putative proteases are secreted. This search identified 95 genes encoding putative secreted proteases. To further narrow this list, we selected genes that were upregulated during the early symptomless stages following *F. graminearum* infection of wheat spikes (at 3 and/or 7 days postinoculation [dpi]) (Brown et al. 2017). These stringent selection criteria identified seven candidate fungal proteases, of which six had been previously tested and shown not to be essential for virulence, at least when individually mutated (Table 1) (Wang et al. 2022; Xiong et al. 2024; Xu et al. 2020). Hence, we focused on functionally characterizing the remaining candidate protease, FGSG_11164 (FGRAMPH1_01G21371).

Analysis of the FGSG_11164 amino acid sequence with InterProScan indicated that this gene encodes a trypsin precursor protein (Fig. 1A). We thus designated FGSG_11164 as *F. graminearum* Trypsin precursor protein 1 (FgTPP1). FgTPP1 encodes a predicted 17-amino acid signal peptide sequence and a trypsin-like serine protease domain (amino acids 27 to 248) (Fig. 1A). Further examination and in silico modeling of the FgTPP1 protein using AlphaFold2 showed that the protein has three predicted catalytic active sites, histidine-67 (His⁶⁷), aspartic acid-112 (Asp¹¹²), and serine-208 (Ser²⁰⁸), as well as a putative substrate binding site consisting of aspartic acid-202 (Asp²⁰²), serine-224 (Ser²²⁴), and glycine-226 (Gly²²⁶) (Fig. 1A and B). Intriguingly, FgTPP1 is also predicted to contain a

chloroplast-targeting peptide sequence (amino acids 62 to 102), suggesting it may localize to chloroplasts (Fig. 1A and B).

The predicted signal peptide of FgTPP1 confers secretion in yeast cells

To test whether the predicted signal peptide of FgTPP1 is functional, we performed a yeast secretion trap assay (Zhou et al. 2020). This assay employs a *suc2* yeast mutant that is unable to grow on media with sucrose as the sole carbon source (Zhou et al. 2020). We fused full-length *FgTPP1*, including its signal peptide sequence, to a truncated *SUC2* gene lacking a signal peptide (*SUC2*²²⁻⁵¹¹), generating a pGAD-*FgTPP1:SUC2*²²⁻⁵¹¹ construct, which was subsequently transformed into a *suc2* yeast mutant. As a negative control, the truncated *SUC2* gene was fused to *FgTPP1* lacking its signal peptide sequence (pGAD-*FgTPP1* Δ SP:*SUC2*²²⁻⁵¹¹). A pGAD-*SUC2*²²⁻⁵¹¹-only construct was used as an additional negative control. As a positive control, we fused the *F. graminearum* effector *FgOSP24*, which was previously shown to be secreted (Jiang et al. 2020), to the truncated *SUC2*²²⁻⁵¹¹ gene and transformed this pGAD-*FgOSP24:SUC2*²²⁻⁵¹¹ construct into a *suc2* yeast mutant. As expected, *suc2* yeast mutants expressing either pGAD-*FgTPP1* Δ SP:*SUC2*²²⁻⁵¹¹ or pGAD-*SUC2*²²⁻⁵¹¹ were unable to grow on yeast synthetic dropout (SD) media supplemented with sucrose as the sole carbon source, indicating that FgTPP1 Δ SP and *SUC2* proteins are not secreted (Fig. 2). Consistent with our hypothesis, *suc2* yeast mutants transformed with either pGAD-*FgTPP1:SUC2*²²⁻⁵¹¹ or pGAD-*FgOSP24:SUC2*²²⁻⁵¹¹ consistently grew on SD media supplemented with glucose or sucrose, demonstrating that the FgOSP24-*SUC2* and FgTPP1-*SUC2* fusion proteins are secreted (Fig. 2). These data thus confirm that the predicted signal peptide from FgTPP1 is indeed functional and confers secretion of FgTPP1 from fungal cells.

FgTPP1 contributes to fungal virulence

Transcriptome data sets obtained from spatial and temporal analyses of the early symptomatic and asymptomatic phases of *F. graminearum* colonization of wheat spikes revealed that the *FgTPP1* gene is strongly induced during the first week of infection (Brown et al. 2017). To assess whether FgTPP1 contributes to fungal virulence, we used a homologous recombination strategy to replace the *FgTPP1* gene with a cassette expressing a bacterial gene conferring resistance to hygromycin B (Supplementary Fig. S1A) (Catlett et al. 2003; King et al. 2017b). Primer combination P20/P21 confirmed deletion of the *FgTPP1* coding sequence in two independent mutant strains (PH-1- $\Delta Fgtp1$ -1 and PH-1- $\Delta Fgtp1$ -3), and primer combinations P16/P17 and P18/P19 confirmed replacement of the *FgTPP1* coding sequence by the hygromycin expression cassette (Supplementary Fig. S1A; Supplementary Table S5). Both $\Delta Fgtp1$ mutants displayed no observable defects in fungal morphology or radial growth when grown on potato dextrose agar plates, including under different stress conditions (Supplementary Fig. S1B). Finally, no noticeable defects were observed in perithecia

Table 1. Summary of the candidate effector proteases expressed during early wheat spikelet infection

Gene ID	Amino acids	Signal peptide	Predicted annotation	Reference(s)
FGSG_00192 (FgPrb1)	533	Yes (1–15)	Cerevisin precursor protein	Xu et al. 2020
FGSG_00806 (FgSLP1)	413	Yes (1–20)	Subtilisin-like peptidase	Xiong et al. 2024; Xu et al. 2020
FGSG_03315 (FgSLP2)	411	Yes (1–20)	Subtilisin-like peptidase	Xiong et al. 2024; Xu et al. 2020
FGSG_08012	390	Yes (1–18)	Proteinase T precursor protein	Xu et al. 2020
FGSG_11164	252	Yes (1–17)	Trypsin precursor protein	This study
FGSG_11472	875	Yes (1–17)	Subtilisin-like peptidase	Xu et al. 2020
FGSG_03467 (FgFly1)	631	Yes (1–23)	Fungalsin metallopeptidase	Wang et al. 2022

formation between the PH-1- $\Delta Fgtp1-1$ mutant and wild-type *F. graminearum* PH-1 strain (Supplementary Fig. S1C).

Next, we investigated whether FgTPP1 is involved in the infection process by performing fungal virulence assays using a top-inoculation approach. In this assay, fungal spores of the PH-1- $\Delta Fgtp1-1$ mutant and wild-type *F. graminearum* PH-1 strain were inoculated into the fifth and sixth spikelets from the top of wheat spikes at anthesis of the susceptible wheat cultivar ‘Bob-white’. Bleached spikelets below the point of inoculation were evaluated at 12 dpi. The PH-1- $\Delta Fgtp1-1$ mutant was able to infect the inoculated spikelets and systemically spread through the spike at a rate similar to that of wild-type *F. graminearum* PH-1 (Fig. 3A). Consistent with the FHB symptoms, no differences

in the number of diseased spikelets throughout the time course and no statistically significant differences in the area under the disease progress curve (AUDPC) were observed between the PH-1- $\Delta Fgtp1-1$ mutant and wild-type *F. graminearum* PH-1 strain (Fig. 3A). To explore further potential virulence defects in the PH-1- $\Delta Fgtp1-1$ mutant, we performed a second inoculation approach, which we refer to as the bottom inoculation assay. Briefly, spores from either the PH-1- $\Delta Fgtp1-1$, PH-1- $\Delta Fgtp1-3$, or wild-type *F. graminearum* PH-1 were inoculated into the first two full-sized spikelets located at the base of a wheat spike at anthesis, and completely as well as partially bleached spikes were recorded at 10 dpi. In this approach, photobleaching of the spikelets may be a consequence of fungal spread

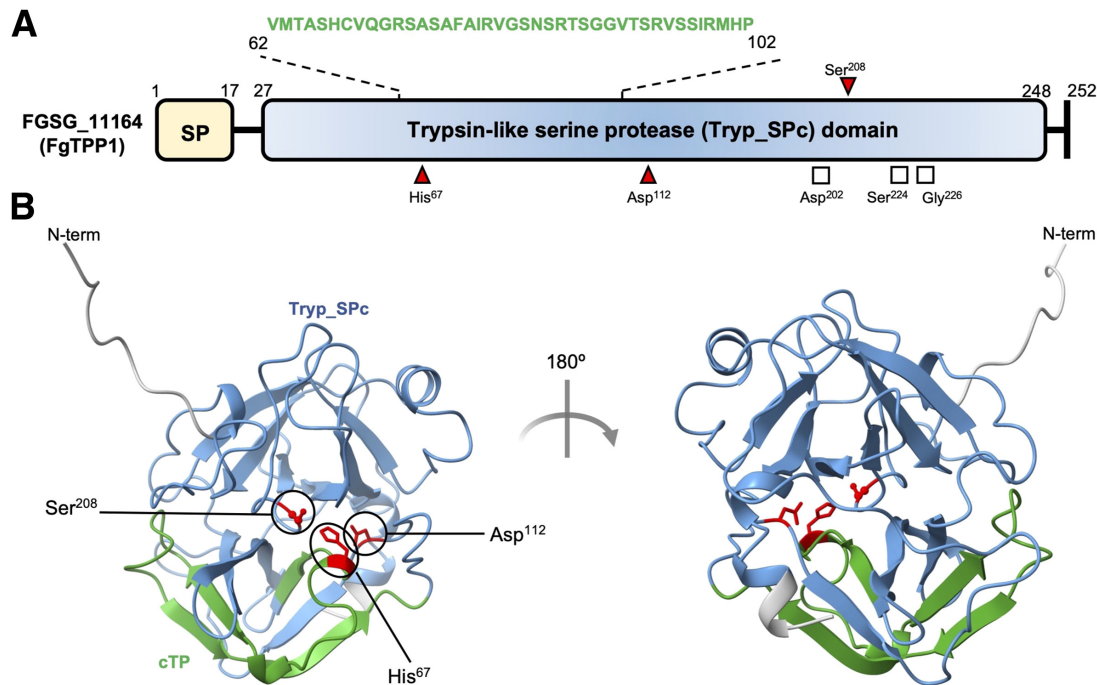


Fig. 1. Schematic illustration and predicted protein structure of FgTPP1 (FGSG_11164). **A**, Schematic representation of the *Fusarium graminearum* candidate effector protease FgTPP1 including the putative signal peptide (SP; amino acids 1 to 17) sequence and the predicted trypsin-like serine protease (Tryp_SPC; amino acids 27 to 248) domain. The predicted chloroplast targeting motif (amino acids 62 to 102) is indicated in green. Putative catalytic active sites (His⁶⁷, Asp¹¹², and Ser²⁰⁸) are indicated by red triangles, and predicted substrate binding sites (Asp²⁰², Ser²²⁴, and Gly²²⁶) are indicated by white squares. Numbers delineate amino acid positions. **B**, The predicted three-dimensional protein structure of FgTPP1 as determined by AlphaFold2. The predicted trypsin-like serine protease domain is indicated in light blue, the chloroplast targeting motif is indicated in green, and the putative catalytic residues are indicated in red. cTP, chloroplast-targeting peptide; N-term, amino terminus.

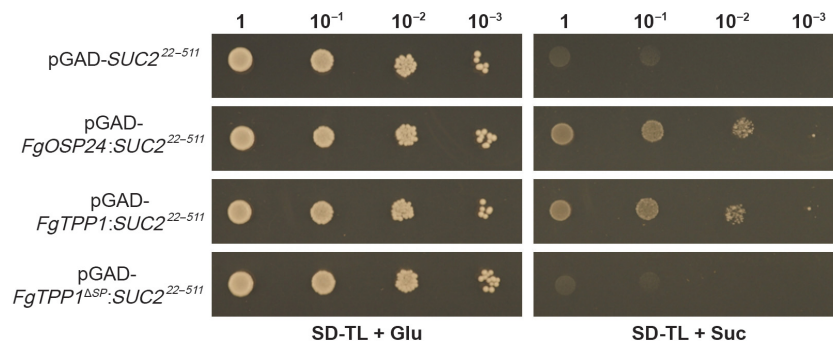


Fig. 2. The FgTPP1 protein encodes a functional secretion signal. A yeast secretion trap assay was performed to test functionality of the predicted signal peptide from FgTPP1 (Zhou et al. 2020). A yeast strain lacking the invertase *SUC2* was transformed with pGAD-*FgTPP1*:*SUC2*²²⁻⁵¹¹, which contains a truncated *SUC2* gene, without its signal peptide (*SUC2*²²⁻⁵¹¹) fused with full-length *FgTPP1*, including its signal peptide sequence, or pGAD-*FgTPP1*^{ΔSP}:*SUC2*²²⁻⁵¹¹, which lacks the predicted signal peptide sequence from *FgTPP1*. As a positive control, the *suc2* yeast mutant was transformed with pGAD-*FgOSP24*:*SUC2*²²⁻⁵¹¹, which contains the full-length *FgOSP24* effector from *Fusarium graminearum* and which was previously shown to be secreted from fungal cells (Jiang et al. 2020). The pGAD-*FgTPP1*^{ΔSP}:*SUC2*²²⁻⁵¹¹ and pGAD-*SUC2*²²⁻⁵¹¹ constructs were used as negative controls. A synthetic dropout (SD) medium lacking tryptophan and leucine (-TL) supplemented with 2% glucose (Glu) was used as the control medium. Images were taken after 4 days of growth, and two independent replicates were performed with similar results. Suc, sucrose.

and/or obstruction of the plant vascular tissue, which, in turn, may lead to cell death in wheat tissues above the inoculation point (Bai and Shaner 2004). Wild-type *F. graminearum* PH-1 caused approximately 50% of the spikes to be fully bleached at 10 dpi, whereas the PH-1- $\Delta Fgtp1-1$ and PH-1- $\Delta Fgtp1-3$ mutant strains induced fewer fully bleached spikes at this time point (18 to 27%) (Fig. 3B). To assess whether this difference was statistically significant, we tested whether the observed data fit a 1:1 ratio. Whereas the data from the wild-type *F. graminearum* PH-1 infection fit this ratio, the data from the mutant infections did not, indicating that these two *tpp1* mutants have reduced virulence (Fig. 3B and C).

To test if partial bleaching of spikes compared with full bleaching was the consequence of either slower disease progression or developmental arrest, additional analyses were performed. The rachis from each partially and fully bleached spike infected with either the wild-type *F. graminearum* PH-1 strain or the $\Delta Fgtp1-1$ mutant was dissected into five segments and plated on synthetic nutrient agar (SNA). Fungal growth in the surrounding agar after 2 days revealed that the *Fusarium* hyphae were alive inside the infected rachises (Fig. 3D). Fully bleached spikes infected with either the $\Delta Fgtp1-1$ mutant or wild-type *F. graminearum* PH-1 strain showed fungal growth on SNA for segment 1 that included the inoculation site and the adjacent segments 2 and 3 (Fig. 3D). Rachis segments 4 and 5 toward the tip of the spike did not show the presence of fungal colonization, despite being fully bleached. In the case of the partially bleached spikes, rachis segments 1 and 2 showed the presence of fungus for all the spikes evaluated, whereas the presence of *Fusarium* hyphae in segment 3 was not always observed (Fig. 3D). A lack of fungal colonization was evident in segments 4 and 5. However, rachis segments 4 and 5 inoculated either with the $\Delta Fgtp1-1$ mutant or wild-type *F. graminearum* PH-1 strain remained either green or predominantly green with just some earlier symptoms of bleaching. Therefore, partially bleached spikes are most likely the consequence of slow disease progression rather than developmental arrest. In addition, the increased number of partially bleached spikes in both $\Delta Fgtp1-1$ mutant strains in comparison with the wild-type *F. graminearum* PH-1 strain suggests that the mutants colonize the spikes more slowly (Fig. 3B and D; Supplementary Fig. S2).

Finally, we tested whether the slower spike colonization was a result of reduced production of the DON mycotoxin. DON concentrations were measured in wheat spikes infected with $\Delta Fgtp1-1$, $\Delta Fgtp1-3$, or the wild-type *F. graminearum* PH-1 strain using the bottom-inoculation approach at 10 dpi. DON values observed for the wild-type *F. graminearum* PH-1 strain were consistent with that of a previous report, when the top-inoculation method was used (Cuzick et al. 2008). Significant differences were not observed between the $\Delta Fgtp1$ mutants when compared with the wild-type *F. graminearum* PH-1 strain, although there was a trend toward slightly reduced DON levels associated with both $\Delta Fgtp1$ mutants (Supplementary Fig. S1D). These results indicate that major changes in in planta DON levels were unlikely to be responsible for the slower colonization observed following inoculation with either $\Delta Fgtp1$ mutant.

To confirm that the observed reduction in FHB disease progression in the bottom-inoculation assay was a result of the absence of FgTPP1, the $\Delta Fgtp1-1$ mutant was complemented with a copy of full-length *FgTPP1*, including its native promoter and terminator, thereby generating the complemented strain PH-1- $\Delta Fgtp1-1::TPP1$. The complementing copy of *FgTPP1* was inserted into a recently described neutral locus in *F. graminearum*, namely Target Site Integration (TSI) locus 1 (Darino et al. 2024). The TSI locus 1 allows for target site integration of different cassettes without affecting either fungal virulence or fungal growth under different conditions. PCR amplifica-

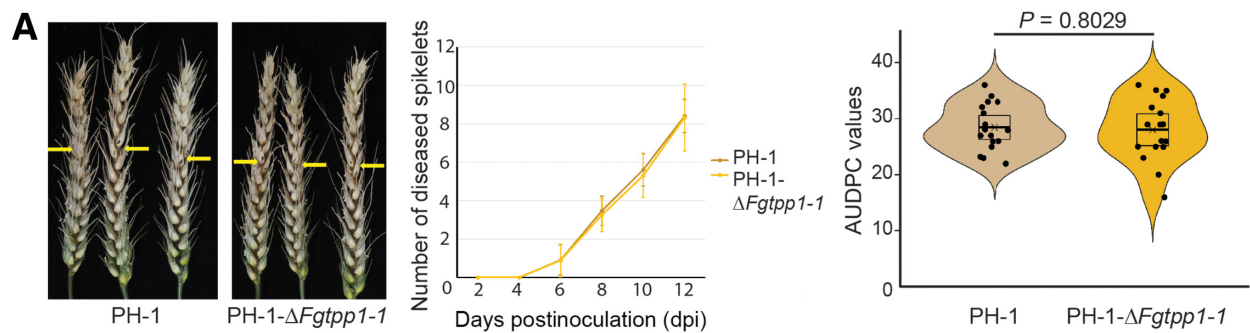
tion confirmed the insertion of a single copy of the cassette, as primer combination P28/P29 amplified the expected 6,123-bp PCR product (Supplementary Fig. S1E; Supplementary Table S5). The PH-1- $\Delta Fgtp1-1::TPP1$ strain did not show observable defects in radial growth or fungal morphology when grown under different stress conditions and, importantly, restored the defect in virulence observed with the PH-1- $\Delta Fgtp1-1$ mutant (Fig. 3B; Supplementary Figs. S1B and S2). Collectively, these data demonstrate that FgTPP1 contributes to *F. graminearum* virulence in wheat spikes.

FgTPP1 accumulates within the stroma of chloroplasts

Analysis of the FgTPP1 amino acid sequence using the deep learning program LOCALIZER (Sperschneider et al. 2017) revealed that FgTPP1 encodes a predicted chloroplast-targeting sequence (amino acids 62 to 102). To test whether FgTPP1 is indeed targeted to chloroplasts, we fused FgTPP1 (without its signal peptide) to the N-terminus of GFP and transiently co-expressed it in *N. benthamiana* with mCherry-tagged Rubisco small subunit transit peptide (RbcS-TP:mCherry), a chloroplast stroma marker protein (Helm et al. 2022; Nelson et al. 2007). Live-cell imaging using laser-scanning confocal microscopy of *N. benthamiana* epidermal cells revealed that FgTPP1:GFP partially localized to the chloroplast stroma, as indicated by an overlap in the fluorescence signal from FgTPP1:GFP and RbcS-TP:mCherry (Fig. 4A). As a control, we expressed free GFP with RbcS-TP:mCherry to exclude the possibility that the apparent chloroplast localization of FgTPP1:GFP was a result of free GFP or chlorophyll autofluorescence. The experiments showed that the fluorescence signal from free GFP did not significantly overlap with the fluorescence signal from the RbcS-TP:mCherry construct (Fig. 4A). We next performed immunoblot analyses to assess protein accumulation and confirm the integrity of the FgTPP1:GFP protein. Intriguingly, these experiments revealed that the FgTPP1:GFP fusion protein consistently produced multiple, distinct protein products, suggesting that the fusion protein may be cleaved prior to or following entry into chloroplasts (Fig. 4B). To further confirm chloroplast localization of FgTPP1, we fused the mCherry fluorescent protein to FgTPP1 (FgTPP1:mCherry) and performed live-cell imaging on chloroplasts isolated from *N. benthamiana*. Confocal microscopy imaging of isolated chloroplasts revealed the mCherry fluorescence signal in some, but not all, chloroplasts (Fig. 4C). Taken together, our results demonstrate that FgTPP1 partially localizes to chloroplasts when transiently expressed in *N. benthamiana*.

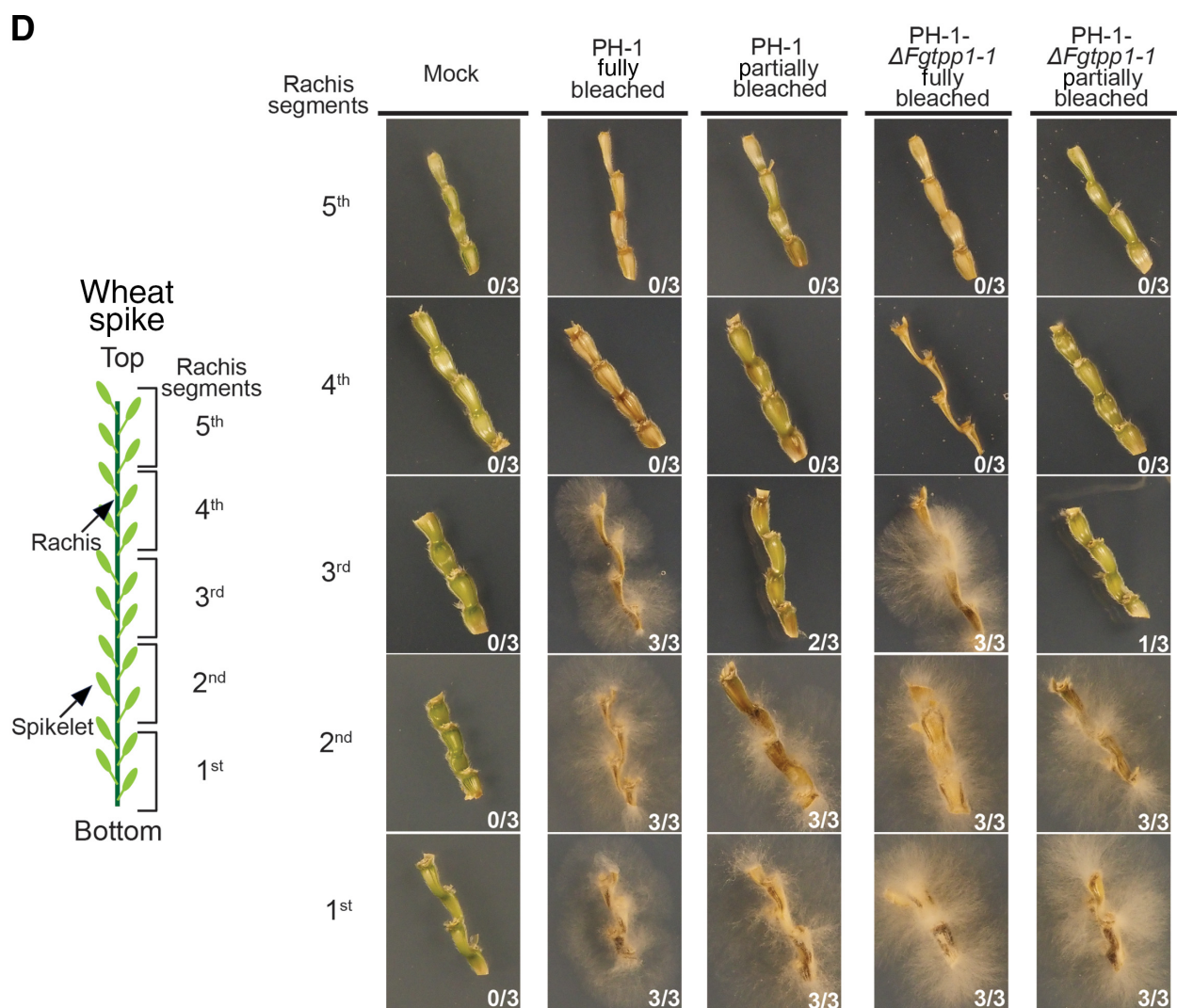
FgTPP1 suppresses cell surface- and intracellular-mediated immune responses

Most pathogen effectors function, at least in part, to suppress host immune responses. Prior to testing whether FgTPP1 can suppress immune signaling, we first confirmed that chitin enhances the accumulation of phosphorylated MAPK protein, specifically the phosphorylation of MAPK3 and MAPK6, which has been linked to immune response signaling downstream of pathogen recognition (Jaiswal et al. 2022). *N. benthamiana* leaves transiently expressing free GFP were infiltrated with either deionized water (mock) or chitin, and at 0, 5, and 10 min following treatment, accumulation of phosphorylated MAPK3 and MAPK6 protein was assessed using immunoblot analyses with MAPK3 and MAPK6 phospho-specific antibodies. These experiments revealed an increase in phosphorylated MAPK3 and MAPK6 protein in response to chitin treatment when compared with the mock control, demonstrating that the increased accumulation of phosphorylated MAPK protein is indeed chitin-mediated (Fig. 5A). To test whether FgTPP1 could attenuate chitin-mediated MAPK signaling, we treated



B

Category	Fungal strain			
	PH-1	$\Delta Fgtpp1-1$	$\Delta Fgtpp1-3$	$\Delta Fgtpp1-1::TPP1$
Partially bleached	31	36	35	25
Fully bleached	28	13	8	19
<i>n</i>	59	49	43	44
Ratio test	<i>P</i> values			
1 : 1	0.6961	1.5×10^{-3}	4×10^{-5}	0.3657



N. benthamiana leaves transiently expressing either free GFP or FgTPP1:GFP with chitin and assessed accumulation of phosphorylated MAPK3 and MAPK6 protein. These experiments revealed that expression of FgTPP1:GFP protein consistently suppressed the accumulation of phosphorylated MAPK3 and MAPK6 in response to chitin relative to the free GFP control (Fig. 5B).

Several effectors from *F. graminearum* have been previously shown to suppress chitin-triggered ROS production (Hao et al. 2019, 2020). To test whether FgTPP1 could also suppress chitin-mediated ROS accumulation, we transiently expressed either free GFP or FgTPP1:GFP in *N. benthamiana* leaves. Plants were subsequently challenged with chitin, and ROS production was monitored over time using a previously optimized luminol-based assay (Rogers et al. 2024). Expression of FgTPP1:GFP consistently attenuated chitin-mediated ROS accumulation when compared with the free GFP control (Fig. 5C). Taken together, our results indicate that FgTPP1 suppresses multiple chitin-mediated immune responses.

Two previously studied effector proteins from *F. graminearum*, namely FgOSP24 and FgNLS1, have been reported to suppress BAX (Bcl-associated X)-induced cell death in *N. benthamiana* and thus likely have a functional role in subverting host immune responses (Hao et al. 2023; Jiang et al. 2020). To test whether FgTPP1 can suppress cell death, we used an allele of the *Arabidopsis* disease resistance protein RPS5, RPS5^{D266E}, which constitutively activates cell death when transiently expressed in *N. benthamiana* (Ade et al. 2007). We fused FgTPP1 to the N-terminus of super yellow fluorescent protein (sYFP) and cloned FgTPP1:sYFP into the dexamethasone-inducible expression plasmid pTA7001 (Qi et al. 2012; Vinatzer et al. 2006). We then transiently co-expressed RPS5^{D266E} with either FgTPP1:sYFP or empty vector and assessed for the suppression of RPS5^{D266E}-mediated cell death 16 h post-dexamethasone induction. These experiments revealed that FgTPP1:sYFP consistently attenuated RPS5^{D266E}-triggered cell death when compared with the empty vector control (Fig. 5D). Collectively, our data demonstrate that FgTPP1 attenuates cell surface-triggered and intracellular-mediated immune responses. Furthermore, the observation that FgTPP1 is secreted; localizes, in part, to chloroplasts; and suppresses immune responses when expressed inside plant cells indicates that FgTPP1 functions inside plant cells and may thus be translocated from the fungus into the host cell during infection.

TPP1 alleles and TPP1 protein haplotypes are conserved among plant-infecting fungi of the Ascomycota phylum

To identify alleles of the *FgTPP1* gene in the *F. graminearum* global population, the nucleotide sequence of *FgTPP1* from the *F. graminearum* PH-1 strain was aligned to the nucleotide sequences of 28 *F. graminearum* isolates collected in 15 countries covering six continents (Supplementary Table S1). Seven alleles of the *FgTPP1* gene were identified (alleles 1 to 7) (Fig. 6A). However, only two protein haplotypes were identified from these 7 alleles (Fig. 6). Protein haplotype I is encoded by alleles 1 to 5, whereas protein haplotype F is encoded by alleles 6 and 7. The difference between the two protein haplotypes resides in amino acid residue 4, where haplotype I possesses an isoleucine, whereas haplotype F possesses phenylalanine (Fig. 6B). This amino acid change resides within the secretion signal, but both protein haplotypes are predicted to be secreted, as determined by SignalP v6.0 (Teufel et al. 2022). Approximately 85.7% of *F. graminearum* strains, including PH-1, have the protein haplotype I, whereas only four recent European strains collected from western bordering countries, including France, Belgium, and Luxembourg, between 2002 and 2008 have protein haplotype F. Next, we calculated the pairwise dN/dS ratios to assess the evolutionary divergence across the protein coding sequences of *FgTPP1* from the 28 *F. graminearum* isolates. The dN/dS ratios were close to zero for all sequences, with a maximum ratio value of 0.01 ± 0.004 observed between the *F. graminearum* isolates pair TPP1_S5A and TPP1_KSU23473 (Supplementary Table S3). These results strongly indicate that the *FgTPP1* gene is under purifying selection within this species. Taken together, our analyses revealed the TPP1 protein sequence is highly conserved among *F. graminearum* isolates collected from diverse geographic regions during the last 50 years, suggesting that it plays a central role in *F. graminearum* survival.

To evaluate the degree of sequence conservation of FgTPP1 in other fungal species, a BlastP search was conducted using the FgTPP1 protein sequence as the query. Homologs of FgTPP1 containing both a predicted secretion signal and a chloroplast transit peptide were identified not only in fungal species from the *Fusarium* genus but also in fungal species belonging to different genera within the Ascomycota phylum (Fig. 7; Supplementary Tables S2 and S3). The FgTPP1 protein appears to be highly conserved (amino acid similarity values between 99 and 81%) in several plant pathogen species residing within the *F. sambucinum* species complex, including *F. culmorum*, *F. pseudo-*

Fig. 3. Deletion of the *FgTPP1* gene reduces fungal virulence in bottom-inoculated wheat spikes. **A**, The PH-1- $\Delta Fgtp1-1$ mutant did not show an observable virulence defect when wheat spikes were inoculated using the top-inoculation method. Yellow arrows indicate inoculation points. Wheat spikes infected with either the $\Delta Fgtp1-1$ mutant (PH-1- $\Delta Fgtp1-1$) or wild-type *F. graminearum* PH-1 strain showed similar disease symptoms (left). The number of diseased spikelets throughout the time courses for the $\Delta Fgtp1-1$ mutant and wild-type *F. graminearum* PH-1 were similar (middle), and the area under the disease progress curve (AUDPC) values calculated for the mutant and wild type did not reveal significant differences (right). Violin plots show distribution of the AUDPC values (black dots), average AUDPC values, and confidence intervals (rectangles) for each fungal strain. The statistical analysis (*t* test) included pooled data from three independent replicates. Each replicate consisted of 12 plants, where 6 plants (one spike per plant) were inoculated with either $\Delta Fgtp1-1$ mutant or wild-type *F. graminearum* PH-1 strains (the total number of plants inoculated was 17 and 18 for the $\Delta Fgtp1-1$ mutant and wild-type *F. graminearum* PH-1 strain, respectively). **B**, The $\Delta Fgtp1$ mutants (PH-1- $\Delta Fgtp1-1$ and PH-1- $\Delta Fgtp1-3$) show a reduction in virulence with the bottom-inoculation method. The observed number of fully and partially bleached spikes fits a 1:1 ratio for the wild-type PH-1 strain, whereas the observed frequencies for the $\Delta Fgtp1$ mutants deviate significantly from the 1:1 ratio ($P < 0.01$). Genetic complementation of the mutant strain $\Delta Fgtp1-1$ with a full copy of the *FgTPP1* gene (PH-1- $\Delta Fgtp1-1::TPP1$) restored the virulence defect, as the complemented strain fits a 1:1 ratio, which is identical to the wild-type *F. graminearum* PH-1 strain. Each replicate consisted of 60 plants. At the inoculation time, plants at anthesis were selected, and a similar number of plants were inoculated with each of the different fungal strains (typically 10 to 14, one spike per plant). Phenotypes were scored at 10 days postinoculation (dpi). The statistical analysis included pooled data from four independent replicates. **C**, Representative wheat spike images from the bottom-inoculation method at 10 dpi. Yellow arrows indicate inoculation points. Fully bleached spikes consist of bleached and light-green spikelets with curved awns along the entire spike. Partially bleached spikes consist of bleached spikelets with curved awns only in the bottom of the spike, whereas the upper spikelets remain dark green with straight awns, as observed in the mock control. **D**, Partially bleached spikes are a consequence of a slow disease progression. Wheat spikes were inoculated with either the PH-1- $\Delta Fgtp1-1$ mutant or wild-type *F. graminearum* PH-1 strain. Rachises from partially and fully bleached spikes were dissected in five segments and plated on plates containing synthetic nutrient agar. The presence of the fungus was observed 2 days after plating. Numbers in the bottom right of each picture indicate the number of segments with fungal presence relative to the total number of spike segments evaluated. Three spikes per condition were tested ($n = 3$).

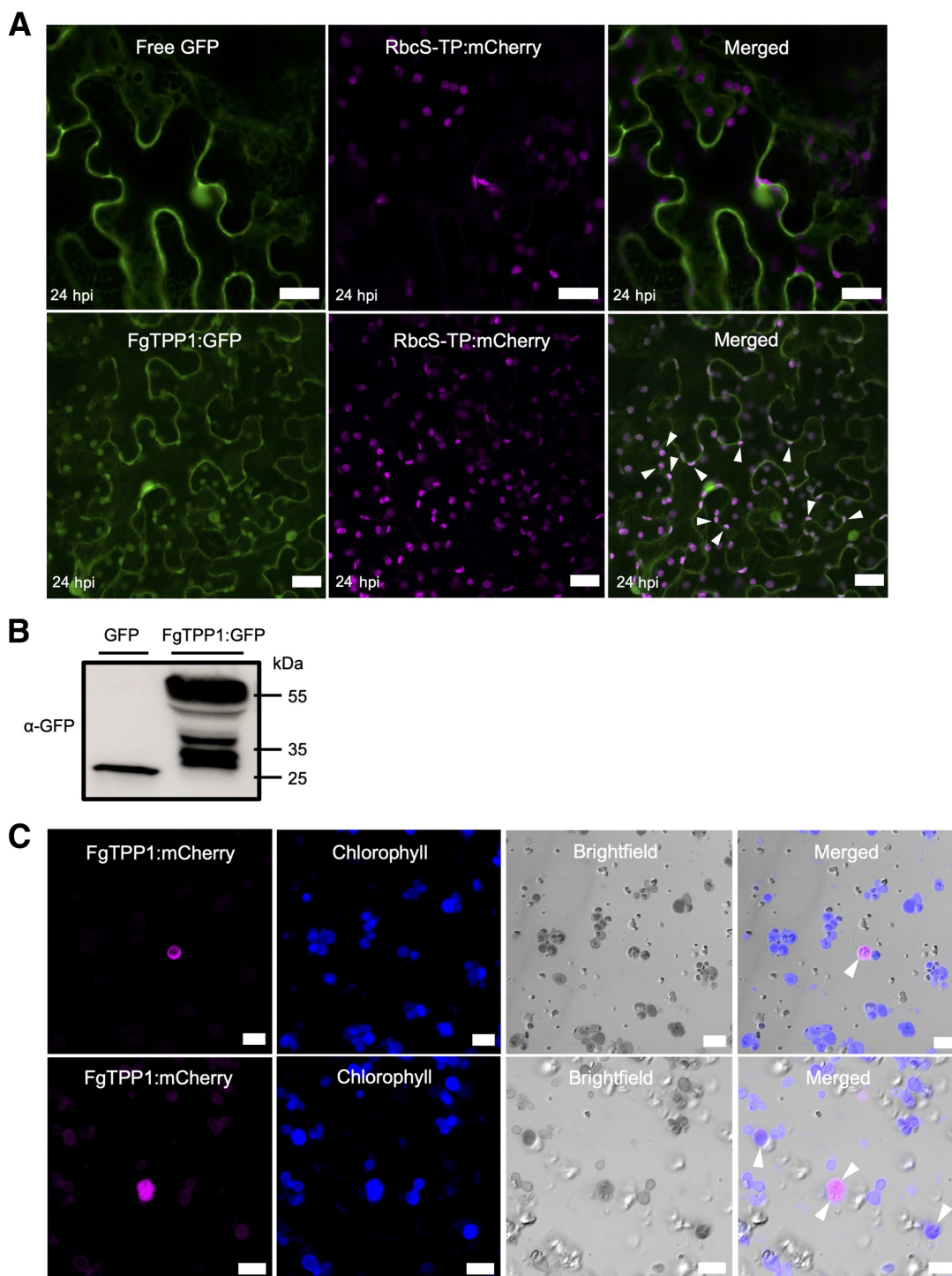


Fig. 4. The FgTPP1:GFP fusion protein targets the chloroplast stroma and nucleio-cytosol when transiently expressed in *Nicotiana benthamiana*. **A**, Green fluorescent protein (GFP)-tagged FgTPP1 (FgTPP1:GFP) localizes to the chloroplast stroma as well as the nucleio-cytosol in *N. benthamiana* epidermal cells. FgTPP1:GFP or free GFP was transiently co-expressed with mCherry-tagged RbcS-TP (RbcS-TP:mCherry) in *N. benthamiana* leaves using *Agrobacterium*-mediated transformation (agroinfiltration). Images were taken 24 h post-agroinfiltration (hpi). mCherry-tagged RbcS-TP was included as a reference for chloroplast localization (Helm et al. 2022). All confocal micrographs shown are of single optical sections. The scale bars represent 20 μm . White arrowheads indicate overlapping GFP and mCherry fluorescence signals. **B**, Immunoblot analysis of the FgTPP1:GFP fluorescent protein fusion. The indicated constructs were transiently expressed in *N. benthamiana* leaves. Total protein was isolated at 24 hpi and analyzed using immunoblotting. α -GFP, anti-GFP. **C**, mCherry-tagged FgTPP1 localizes to chloroplasts isolated from agroinfiltrated *N. benthamiana*. Leaf tissue transiently expressing FgTPP1:mCherry was harvested at 24 hpi and homogenized in cold isolation buffer. Chloroplasts were isolated as described in the Materials and Methods section and imaged using laser-scanning confocal microscopy. Chlorophyll autofluorescence (in blue) was used as a marker for chloroplasts. White arrowheads indicate overlapping mCherry and chlorophyll fluorescence signals. Confocal micrographs from two independent biological replicates are shown in the top and bottom panels. The scale bars shown represent 10 μm .

graminearum, *F. sporotrichioides*, *F. langsethiae*, *F. venenatum*, and *F. poae* (Armer et al. 2024a; Waalwijk et al. 2018). In addition, the FgTPP1 protein is conserved in other plant-pathogenic *Fusarium* species (similarity values between 87 and 71%), such as *F. equiseti*, *F. fujikuroi*, *F. verticillioides*, *F. oxysporum*, and *F. tricinctum*, that belong to different *Fusarium* species complexes (Fig. 7; Supplementary Table S2). Some *Fusarium* species, such as *F. sarcochroum*, *F. torreyae*, *F. tricinctum*, and *F. avenaceum*, possess two copies of the *TPP1* gene (Supplementary Table S2). Finally, FgTPP1 is also conserved (similarity values between 64 and 52%) in fungal species from different genera within the Ascomycota phylum (Supplementary Table S4). Most of these species have been classified either as plant pathogenic (*Alternaria alternata* and *Verticillium dahliae*) or plant endophytic (*Colletotrichum tofieldiae* and *Alternaria rosae*) (Fig. 7; Supplementary Table S4). Multiple copies of TPP1 homologs were also discovered in species residing in the *Alternaria* genus. Whereas *A. panax* and *A. rosae* have 2 copies of *TPP1*, 3 copies were found in *A. alternata* and *A. burnsii*. The strong conserva-

tion of *TPP1* across a wide range of ascomycete plant pathogens and endophytes suggests that TPP1 may play a conserved role(s) in plant colonization.

Discussion

In this study, we examined the functional roles and immune-suppressing properties of a putative effector protease from *F. graminearum*, FgTPP1, which was previously shown to be upregulated during early stages of wheat spike infection by *F. graminearum*, suggesting that it plays a role in fungal colonization and infection of the wheat spike. Consistent with this, the virulence of $\Delta Fgtp1$ mutants was reduced when compared with the wild-type *F. graminearum* PH-1 strain using a bottom-inoculation method. In this infection assay, *F. graminearum* colonizes the wheat rachis and vascular tissue, thereby inhibiting nutrient and water transport to the systemic, noninfected spikelets, resulting in bleaching of the wheat spike (Bai and Shaner 2004). During the bottom-inoculation method, we

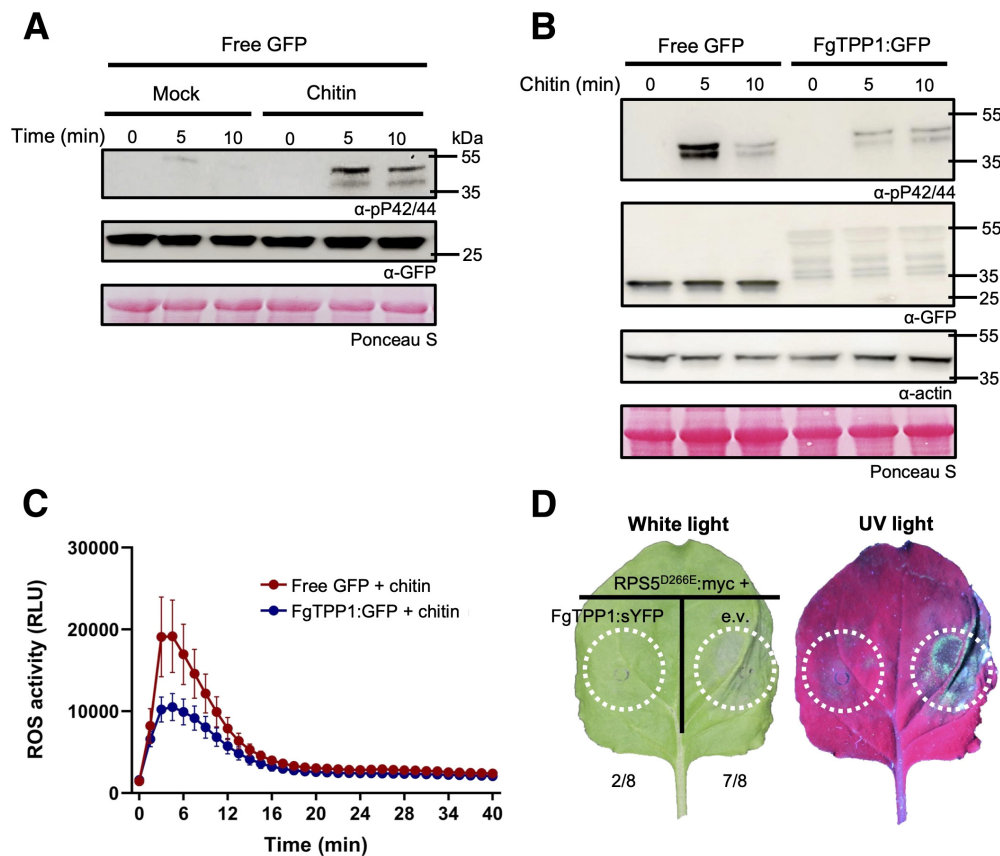


Fig. 5. FgTPP1 suppresses cell surface-triggered and intracellular-mediated immune responses. **A**, MAPK3 and MAPK6 phosphorylation is induced upon chitin treatment. *Nicotiana benthamiana* leaves transiently expressing free green fluorescent protein (GFP) (to control for the presence of *Agrobacterium tumefaciens*) were agroinfiltrated using a needleless syringe. Forty-eight hours following agroinfiltration, leaves were infiltrated with chitin (5 μ g/ml of chitin [hexamer]) and leaf discs (10-mm diameter) harvested at the indicated time points for protein extraction. Anti-phospho-P42/44 antibodies (α -pP42/44) were used to detect phosphorylated MAPK3 and MAPK6. Mock-treated leaves were infiltrated with deionized water. Ponceau S staining was used as a loading control. α -GFP, anti-GFP. **B**, Chitin-induced accumulation of phosphorylated MAPK3 and MAPK6 is attenuated by FgTPP1. The indicated constructs were transiently expressed in *N. benthamiana*. Forty-eight hours after agroinfiltration, leaves were infiltrated with chitin (5 μ g/ml of chitin [hexamer]), total protein was extracted at the indicated time points, and immunoblotting was performed using the indicated antibodies. *N. benthamiana* actin and Ponceau S staining were used as loading controls. **C**, Transient expression of FgTPP1:GFP attenuates chitin-induced reactive oxygen species (ROS) burst in *N. benthamiana*. FgTPP1:GFP or free GFP was transiently expressed in *N. benthamiana*. Forty-eight hours after agroinfiltration, *N. benthamiana* leaf discs (5-mm diameter) were collected and treated with chitin (5 μ g/ml of chitin [hexamer]), and relative luminescence (RLU) was monitored for 40 min using a previously optimized luminol-based assay (Rogers et al. 2024). **D**, Suppression of RPS5^{D266E}-mediated cell death by FgTPP1 in the *N. benthamiana* leaves. *N. benthamiana* leaves were co-infiltrated with *A. tumefaciens* strains carrying myc-tagged RPS5^{D266E} (OD₆₀₀ = 0.15), FgTPP1 fused to the N-terminus of super yellow fluorescent protein (FgTPP1:sYFP; OD₆₀₀ = 0.3), or empty vector (e.v.; OD₆₀₀ = 0.3). Forty-eight hours following agroinfiltration, *N. benthamiana* leaves were sprayed with 50 μ M dexamethasone to induce protein expression. *N. benthamiana* leaves were assessed for cell death and photographed under white and ultraviolet (UV) light 16 h post-transgene induction. Fractions indicate the number of leaves with observable hypersensitive response such as cell death/the total number of leaves agroinfiltrated. Experiments were performed three independent times with similar results.

observed fully bleached spikes and curved awns during the onset of spikelet bleaching (spike discoloration), which may be used as an additional criterion to categorize infection severity. Furthermore, these symptomatic characteristics allowed us to distinguish between fully bleached and partially bleached spikes, thereby affording us the opportunity to more consistently phenotype FHB disease progression. It is worth noting the importance

of the time point at which the inoculated plants were evaluated. We have observed that disease symptoms in partially bleached spikes progress over time, and most of the partially bleached spikes become fully bleached at 13 dpi. Earlier scoring times (i.e., before 10 dpi) did not generate data sets that were able to distinguish between the $\Delta Fgtp1$ mutants and the wild-type *F. graminearum* PH-1 strain, as most of the infected spikes were

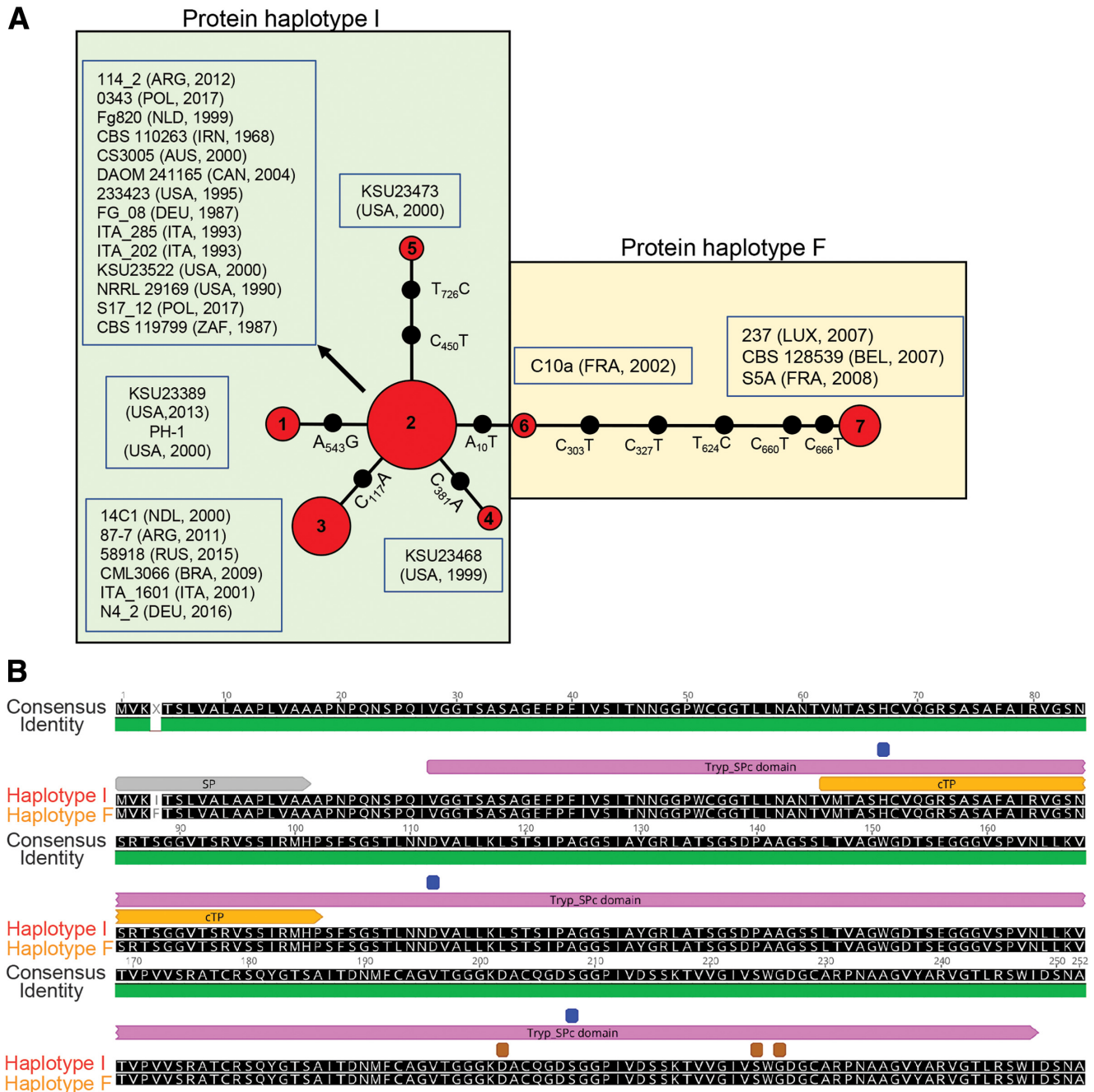


Fig. 6. *TPP1* alleles and *TPP1* protein haplotypes in *Fusarium graminearum* isolates collected globally. **A**, Allele networks for the *FgTPP1* coding sequences from 28 *F. graminearum* isolates collected worldwide. Red circles represent one allele, and the number within each of the red circles represents the allele number. Each black circle represents the number of mutations between adjacent alleles. The mutated bases in alleles 2 to 7 are compared with allele 1. Five alleles (alleles 1 to 5) encode the protein haplotype isoleucine (I), and two alleles (alleles 6 and 7) encode protein haplotype phenylalanine (F). Haplotype networks were generated in POPART using a minimum spanning network. The country of origin and year during which each isolate was collected are given between brackets. ARG, Argentina; AUS, Australia; BEL, Belgium; BRA, Brazil; CAN, Canada; DEU, Germany; FRA, France; IRN, Iran; ITA, Italy; LUX, Luxembourg; NDL, the Netherlands; POL, Poland; RUS, Russia; USA, the United States; and ZAF, South Africa. **B**, Amino acid alignment of *FgTPP1* for both protein haplotypes. The blue and brown squares represent predicted active sites and binding sites, respectively, between haplotypes I and F. Annotations in gray, light violet, and orange lines represent the predicted signal peptide sequence (SP), the predicted trypsin domain (Tryp_SPC), and the predicted chloroplast-targeting peptide (cTP), respectively. Isoleucine-4 (haplotype I) and phenylalanine-4 (haplotype F) indicate the difference between the two protein haplotypes. Functional secreted signals were predicted for both haplotypes using SignalP v6.0 (Teufel et al. 2022).

partially bleached. Under our conditions, the transition from partially to fully bleached spikes occurs very quickly, typically over a 1- to 2-day time window, thus making it rather challenging to count diseased spikelets accurately throughout this brief phase of the infection time course. Therefore, this brief phase affects the accuracy of the AUDPC values. Instead, we have observed that wheat spikes infected with wild-type *F. graminearum* PH-1 follow a 1:1 ratio (partially/fully bleached spikes) at 10 dpi. This ratio can be used to establish if the $\Delta Fgtp1$ mutants deviate from the frequencies of partially/fully bleached spikes observed for the PH-1 strain. In contrast to the bottom-inoculation method, the top-inoculation approach consists of counting the number of diseased spikelets below the inoculation point and is often reliable when there are significant differences between mutant and wild-type *F. graminearum* strains, such as the recently characterized

cell wall stress tolerance $\Delta Knr4$ mutant (Kroll et al. 2025). However, distinguishing between an infected and uninfected wheat spikelet can be challenging using the top-inoculation method, especially during the early stages of spikelet infection. Consequently, reduced virulence phenotypes are often difficult to reliably phenotype, especially when subtle. In our study, we did not observe a reduction in fungal virulence with the $\Delta Fgtp1-1$ mutant when using the top-inoculation method and the wheat cultivar Bobwhite. Our results presented here are also inconsistent with that of Menke (2011) who, in a non-peer-reviewed study, showed that a $\Delta Fgtp1$ mutant strain exhibited a subtle reduction in fungal virulence using the top-inoculation method and the wheat cultivar 'Norm'. Specifically, Menke (2011) reported that the number of diseased spikelets per infected spike with the wild-type *F. graminearum* PH-1 strain was 7.7 ± 0.3 ,



Fig. 7. Phylogenetic tree of TPP1 protein homologs present in *Fusarium* species and other ascomycete fungi. *Aspergillus pseudocaelatus* was used as an outgroup. Branches with an asterisk (*) are supported by bootstrap value and/or posterior probability with minimum score 70/0.7. Multiple paralogs of TPP1 were present in single isolates of ¹*Alternaria panax*, ²*A. alternata*, ³*A. burnsii*, ⁴*A. rosae*, ⁵*F. sarcochroum*, ⁶*F. torreyae*, ⁷*F. avenaceum*, and ⁸*F. tricinctum*.

whereas the number of disease spikelets per spike infected with the $\Delta Fgtp1$ mutant was 7.2 ± 0.2 , a 6% reduction in fungal colonization. Collectively, our experiments using different infection methods suggest that the bottom-infection method is likely more sensitive to subtle virulence defects and could be used to further analyze *F. graminearum* mutants that do not show significant virulence defects using the top-inoculation method.

Approximately seven predicted proteases, some of which are highly expressed during in planta fungal growth, have been individually deleted in *F. graminearum*. However, only one *F. graminearum* mutant (FGSG_00192; FgPrb1) showed a significant reduction in fungal pathogenicity (Xu et al. 2020). This result may suggest that either candidate proteases are not directly involved in fungal pathogenicity, or fungal proteases may be functionally redundant, and, therefore, single deletion mutants are not sufficient to produce a strong reduction in fungal pathogenicity. For example, single gene deletions of two subtilisin-like protease genes, *FgSLP1* (FGSG_00806) and *FgSLP2* (FGSG_03315), did not significantly affect fungal virulence in wheat spikes when compared with the wild-type *F. graminearum* PH-1 strain (Xu et al. 2020). However, simultaneous deletion of both *FgSLP1* and *FgSLP2* resulted in a significant reduction in fungal virulence, indicating that *FgSLP1* and *FgSLP2* are functionally redundant and complement each other during pathogenesis (Xiong et al. 2024). In addition to subtilisin-like proteases, *F. graminearum* expresses other putative proteases during in planta growth that attenuate plant defense responses, such as the serine carboxypeptidase FgSCP (FGSG_08454) (K. Liu et al. 2024). The FgSCP protease from *F. graminearum* suppresses cell death, when transiently expressed in *N. benthamiana*, positively regulates the expression of DON biosynthesis and plays a direct role in *F. graminearum* pathogenicity in wheat as well as maize (K. Liu et al. 2024). Similar to FgSCP1 and FgTPP1, the aspartic protease FolAsp, from *F. oxysporum* f. sp. *lycopersici*, was recently shown to inhibit hypersensitive response-like cell death as well as suppress PAMP-mediated ROS burst in *N. benthamiana* (Wang et al. 2023). Importantly, FolAsp is involved in *F. oxysporum* f. sp. *lycopersici* pathogenicity in tomato seedlings (Wang et al. 2023). The observation that *F. graminearum* expresses and secretes multiple proteases that suppress plant immunity suggests that deleting additional, functionally redundant proteases in the $\Delta Fgtp1$ mutant may further reduce fungal virulence.

Our finding that FgTPP1 localizes, in part, to the chloroplast stroma suggests *F. graminearum* may modulate chloroplast-mediated immune responses during fungal infection. It is worth noting that biosynthesis of the defense phytohormone salicylic acid (SA) occurs, in part, within chloroplasts, and SA production is important for defense against biotrophic and hemibiotrophic pathogens (Ding and Ding 2020; J. Liu et al. 2024). In addition to salicylic acid, chloroplasts also produce ROS, which often function as signaling molecules to propagate immune responses against pathogens (Galvez-Valdivieso and Mullineaux 2010; J. Liu et al. 2024). Considering the importance of SA production and ROS accumulation during plant-pathogen interactions, it stands to reason that downregulation of chloroplast functions could potentially interfere with production of defense signaling molecules (Kretschmer et al. 2020). Indeed, several filamentous fungal pathogens have evolved effector proteins that localize to chloroplasts to subvert chloroplast-derived defense responses (Figueroa et al. 2021; Littlejohn et al. 2021). For example, the wheat stripe rust pathogen *Puccinia striiformis* f. sp. *tritici* expresses and secretes the Pst_12806 effector inside host cells, where it subsequently localizes to host chloroplasts and interacts with the chloroplast iron-sulfur protein, TaISP (Xu et al. 2019). The poplar rust fungus *Melampsora larici-populina* encodes three chloroplast-targeting proteins (CTP1, CTP2, and

CTP3) that, similar to FgTPP1, contain chloroplast-targeting sequences and localize to the stroma of chloroplasts in *N. benthamiana* (Petre et al. 2015, 2016). Although we hypothesize that the immune-suppressing activities of FgTPP1 may be a result of its localization to chloroplasts, our data do not rule out the possibility that FgTPP1 may function in the nucleocytosol to suppress immunity. Hence, future work will focus on testing whether the subcellular localization of FgTPP1 is important for its immune-suppressing activities, identifying host proteins from wheat that interact with this candidate effector protease, and determining what effect such interactions have on facilitating *F. graminearum* infection and FHB disease development.

One of the reasons we have been researching effector proteases from *F. graminearum* is the potential to bioengineer novel recognition specificities of such proteases using decoy substrates. Many wheat and barley cultivars encode for the nucleotide-binding leucine-rich repeat (NLR) disease resistance gene *AvrPphB response 1* (*Pbr1*), which mediates recognition of the AvrPphB protease from *Pseudomonas syringae* (Carter et al. 2019; Jaiswal et al. 2023). AvrPphB is known to target receptor-like cytoplasmic kinases (RLCKs) in subfamily VII, which includes PBS1, from *Arabidopsis* (Shao et al. 2003; Zhang et al. 2010). We have previously shown that the AvrPphB cleavage site within PBS1 can be replaced with cleavage sequences for other pathogen-secreted proteases, including viral proteases, which then confers recognition and resistance to the pathogens expressing those proteases, including soybean mosaic virus and turnip mosaic virus (Helm et al. 2019; Kim et al. 2016). By extension, it may be feasible to introduce genetic-based resistance to *F. graminearum* by bioengineering a barley and wheat RLCK such that, when proteolytically cleaved by FgTPP1, activates PBR1-mediated immunity. Although there are no reported NLR-based resistance genes against *F. graminearum*, we predict such NLR-mediated immune responses will be effective at conferring resistance to this fungal pathogen. For example, the tomato NLR immune receptor I2 was shown to confer recognition and resistance to *F. oxysporum* f. sp. *lycopersici* (Simons et al. 1998). A major goal for us going forward will be the identification of the preferred cleavage site sequence for FgTPP1, which would then enable us to generate decoy substrates that, when cleaved, would activate immune responses. If successful, the bioengineering of barley and wheat RLCK decoy proteins is expected to contribute to the development of improved crop protection strategies for *F. graminearum*. Importantly, we would expect such resistance to be quite durable, as *FgTPP1* is conserved among all sequenced *F. graminearum* genomes, and the gene appears to be under purifying selection within the *F. graminearum* species, which indicates that it likely has a central role in the *F. graminearum* life cycle. Furthermore, the conservation of *FgTPP1* across fungal plant pathogens from the Ascomycetes phylum suggests that it may be possible to bioengineer resistance to fungal plant diseases of many different crops using the same approach.

Materials and Methods

Strains, media, and culture

Fusarium graminearum wild-type strain PH-1 (Cuomo et al. 2007) was used as the background strain to generate the $\Delta Fgtp1$ mutant strains. The wild-type PH-1, PH-1- $\Delta Fgtp1$ mutant strains, and complementation strain PH-1- $\Delta Fgtp1$ -1::TPP1 were grown on SNA (0.1% KH₂PO₄, 0.1% KNO₃, 0.1% MgSO₄ × 7 H₂O, 0.05% KCl, 0.02% glucose, 0.02% saccharose, and 2% agar) under constant ultraviolet and white light illumination. Conidiation was induced by adding 3 ml of TB3 liquid medium (0.3% yeast extract, 0.3% casamino acid, and 20% sucrose) to SNA plates containing 7-day-old fungal mycelia. Conidia were harvested 2 days later in sterile water

and stored at -80°C as described previously (Brown et al. 2011). *Escherichia coli* strain DH5 α was used for plasmid construction. *E. coli* transformants were selected on Luria-Bertani agar supplemented with either 25 $\mu\text{g/ml}$ of gentamicin or 100 $\mu\text{g/ml}$ of ampicillin. Defects in radial growth in the mutant and complemented strains compared with PH-1 were evaluated under different stress conditions as previously described (Darino et al. 2024). Briefly, 25 ml of half-strength potato dextrose agar was mixed with different stress-inducing agents, such as membrane stresses (Congo Red [50 $\mu\text{g/ml}$], Calcofluor [100 $\mu\text{g/ml}$], and 0.02% Tergitol) and salt stress (1 M NaCl), and poured into squares plates. The strains were also evaluated on SNA. Three tenfold serial dilutions were prepared from a water stock containing 10^6 fungal conidia/ml. Each spore dilution was spotted onto agar plates in 20- μl droplets. Plates were incubated at room temperature under dark conditions for the entirety of the experiment. Photographs were taken at 2 dpi. The experiment was repeated twice. Defects in perithecia induction and formation between the PH-1- $\Delta Fgtp1$ -1 mutant strain and PH-1 were evaluated on carrot agar medium following the protocol described by Cavinder et al. (2012). Photographs were taken 9 days after inoculation of the fungal strains on plates containing carrot agar. The experiment was repeated three independent times.

Plant growth conditions

Seeds of *N. benthamiana* were grown in pots containing Berger Seed and Propagation Mix supplemented with Osmocote slow-release fertilizer (14-14-14) and maintained in a growth chamber with a 16:8-h photoperiod (light/dark) at 24°C in the light and 20°C in the dark, with average light intensities at plant height of 120 $\mu\text{mol}/\text{m}^2/\text{s}$.

Spring wheat cultivar Bobwhite seedlings were grown in pots containing Rothamsted mix soils with 50% the standard fertilizer rate and maintained in a controlled environment room with a 16:8-h photoperiod (light/dark) under white-based LEDs with far-red addition (HeliosPEC R40F Flex) with average light intensities of 300 $\mu\text{mol}/\text{m}^2/\text{s}$ and 65% relative humidity. Temperatures during light/dark conditions were 20 and 18°C , respectively (Darino et al. 2024).

Prediction of the FgTPP1 protein structure using AlphaFold2

The protein structure of FgTPP1 (without the predicted signal peptide sequence) was predicted using ColabFold v1.5.2: AlphaFold2 using MMseqs2 with default parameters as previously described (Mirdita et al. 2022; Rogers et al. 2024). The predicted protein structure with the highest confidence (pLDDT) score as determined by AlphaFold2 (i.e., ranked_0.pdb) was captured and visualized using ChimeraX-1.5 (Meng et al. 2023).

Yeast secretion trap assay for testing signal peptide function

Secretion of different *F. graminearum* proteins was tested in yeast using the yeast secretion trap assay as previously described by Zhou et al. (2020) with slight modifications. Briefly, secretion signals from FgTPP1 and FgOSP24 were predicted using SignalP v6.0 (Teufel et al. 2022). Full-length coding sequences of FgTPP1, FgOSP24, and FgTPP1 without the predicted secretion signal (FgTPP1 ΔSP) were PCR-amplified using primer combinations P1/P2, P3/P4, and P5/P2, respectively, using complementary DNA generated from wheat floral tissue infected with *F. graminearum* wild-type strain PH-1 as the template. The resulting PCR products were cloned into the pDONR207 plasmid using a Gateway cloning approach (Invitrogen). Donor clones containing pDONR207-FgTPP1, pDONR207-FgOSP24, and pDONR207-FgTPP1 ΔSP were recombined with the destination vector pGAD-GW-SUC2 $^{22-511}$ using the Gateway cloning

system (Invitrogen) to generate the following constructs: pGAD-FgTPP1:SUC2 $^{22-511}$, pGAD-FgOSP24:SUC2 $^{22-511}$, and pGAD-FgTPP1 ΔSP :SUC2 $^{22-511}$. Each construct was transformed into a yeast sucrose invertase (*suc2*) mutant using a yeast transformation kit following the manufacturer's instructions (Yeast Transformation Kit, Sigma-Aldrich). The *suc2* mutant is unable to secrete the SUC2 protein and thus cannot grow on media containing sucrose as the sole carbon source. Transformants were plated on yeast SD media lacking tryptophan and leucine (-TL) supplemented with 2% glucose (Glu). The lack of tryptophan and leucine is to select positive transformants of the yeast *suc2* mutant containing the different constructs. Plates were incubated at 30°C for 3 days. Yeast transformants were verified by PCR amplification to determine the presence of the fusion proteins using the primer combination P6 and P7. Positive clones were inoculated into liquid SD-TL 2% Glu media and incubated at 30°C overnight with slight agitation (180 rpm). Following overnight incubation, liquid cultures were adjusted to an optical density (OD) at 600 nm (OD $_{600}$) of 1.0 and centrifuged at 4,000 rpm for 2 min to remove the growth media. Yeast pellets were resuspended in sterile water, and three tenfold serial dilutions for each transformant were prepared. Five microliters of each dilution was spotted onto plates containing SD-TL supplemented with either 2% Glu or 2% sucrose. Plates were incubated at 30°C for 4 days. Empty vector pGAD-GW-SUC2 $^{22-511}$ was used as a negative control. The experiment was repeated twice.

Deletion of tpp1 and complementation in F. graminearum

The "split-marker" approach utilizing two overlapping DNA fragments was used to delete the FgTPP1 gene from the *F. graminearum* PH-1 strain (Catlett et al. 2003; King et al. 2017b). Briefly, two plasmids, pEK01 and pEK02, were designed to delete FgTPP1. The vector pEK01 contained a 1,000-bp fragment upstream of the start codon of the FgTPP1 gene (P $_{\text{TPP1}}$) followed by a partial sequence of the hygromycin B resistance cassette (Hyg $_{1-761}$). P $_{\text{TPP1}}$ was PCR-amplified from *F. graminearum* PH-1 genomic DNA using primers P8 and P9, and the Hyg $_{1-761}$ fragment was PCR-amplified from the pHyg1.4 vector using primers P10 and P11 (Urban et al. 2003). The vector pEK02 contained a fragment of the hygromycin B resistance cassette (Hyg $_{296-1027}$) followed by a 1,000-bp fragment of the terminator region of FgTPP1 downstream of the stop codon (T $_{\text{TPP1}}$). Primers P12 and P13 were used to PCR-amplify T $_{\text{TPP1}}$ from PH-1 genomic DNA, and primers P14 and P15 were used to PCR-amplify the fragment Hyg $_{296-1027}$ from the pHyg1.4 vector. Gibson assembly was used to ligate the PCR fragments (P $_{\text{TPP1}}$ with Hyg $_{1-761}$ and Hyg $_{296-1027}$ with T $_{\text{TPP1}}$) into the pGEM-T Easy vector to generate plasmids pEK01 and pEK02, respectively. The two plasmids share a 466-bp overlapping region of the Hyg cassette to allow recombination during the transformation step.

To proceed with the transformation step, PCR products containing the P $_{\text{TPP1}}$ -Hyg $_{1-76}$ and Hyg $_{296-1027}$ -T $_{\text{TPP1}}$ were PCR-amplified using HotStart polymerase and primer combinations P8/P11 and P14/P13, respectively. Then, 5- μl aliquots of 2 $\mu\text{g/ml}$ from each PCR product were combined and used to transform 1×10^8 protoplasts generated from *F. graminearum* PH-1 according to the protocols described by Hohn and Desjardins (1992) and King et al. (2017b). Transformants were selected on regeneration media (0.2% yeast extract, 0.2% casein-hydrolysate [N-Z-Amine A], 0.7% agarose, and 0.8 M sucrose) containing 75 $\mu\text{g/ml}$ of hygromycin. Well-spaced transformants were selected using sterile wooden toothpicks and transferred to 6-well plates containing SNA with 75 $\mu\text{g/ml}$ of hygromycin. To extract genomic DNA, transformants were grown on yeast peptone dextrose broth containing 75 $\mu\text{g/ml}$ of Hyg B, and DNA was extracted according to the method described by Rudd et al.

(2010). PCR diagnostic tests were performed to confirm the correct insertion of the Hyg cassette into the *TPP1* locus (primer combinations P16/P17 and P18/P19) and to test for *FgTPP1* coding sequence replacement (primer combination P20/P21) (King et al. 2017b).

The $\Delta Fgtpp1-1$ mutant was complemented with the coding sequence of *FgTPP1* at the TSI locus 1 (Darino et al. 2024). A DNA fragment containing the *FgTPP1* coding sequence, including the promoter and terminator regions of *FgTPP1* ($P_{tpp1}-TPP1-T_{tpp1}$) was PCR-amplified from genomic DNA of PH-1 using primer combination P22 and P23. The PCR product was cloned into the Fg vector as previously described (Darino et al. 2024). The Fg vector contains a fragment of the geneticin resistance cassette followed by the right border (RB) of the TSI locus 1 (*geneticin*₁₋₆₆₄-RB). Between the RB and the partial sequence of the geneticin cassette, there is a cloning site adapted to the Golden Gate cloning approach (Engler et al. 2009). Integration into the TSI locus 1 was accomplished following an adaptation of the split-marker approach (Darino et al. 2024). Briefly, a PCR product containing the partial fragment of the geneticin resistance cassette followed by the $P_{tpp1}-TPP1-T_{tpp1}$ region and the RB of the TSI locus 1 (*geneticin*₁₋₆₆₄- $P_{tpp1}-TPP1-T_{tpp1}$ -RB) was PCR-amplified from the Fg vector using primer combination P24 and P25. A second PCR product containing the left border (LB) of the TSI locus 1 followed by the split fragment of the geneticin resistance cassette (*geneticin*₇₉₅₋₁₂₈) was amplified from the pJET-LB-*geneticin* vector using primer combination P26 and P27. Both PCR products possess an overlapping region of 536 bp to allow for homologous recombination. The PCR products were adjusted to a final concentration of 2 $\mu\text{g}/\mu\text{l}$. Finally, 5 μl of each PCR product was aliquoted and mixed. The mixture of PCR products was used to transform *F. graminearum* protoplasts prepared from the PH-1- $\Delta Fgtpp1-1$ mutant following the protocol described above. Transformants were selected on SNA plates containing 75 $\mu\text{g}/\text{ml}$ of geneticin. To test for single insertion of the expression cassette into the TSI locus 1, a diagnostic PCR spanning from outside the recombination region was performed using primer combination P28 and P29. A transformant with an amplicon of 6,123 bp was selected as the positive transformant. The primers used in this study are listed in Supplementary Table S5.

FHB virulence assays

The susceptible spring wheat cultivar Bobwhite, sourced from the International Maize and Wheat Improvement Centre (CIM-MYT, Mexico), was inoculated at anthesis following the top inoculation approach as previously described by Wood et al. (2020) with slight modifications. Briefly, two spikelets per wheat spike were inoculated, using 4 to 7 plants per fungal strain and only the first spike per plant. The 14th and 15th spikelets, counting up from the bottom, were point-inoculated with 5 μl of 1×10^5 conidia/ml of either PH-1- $\Delta Fgtpp1-1$ or wild-type *F. graminearum* PH-1. As a control, wheat cultivar Bobwhite plants were inoculated with sterile deionized water. Inoculated wheat plants were incubated under high humidity conditions (above 80%) for 48 h, with an initial 24 h in the dark. FHB disease was scored by counting the number of infected spikelets below the point of inoculation every 2 days until 12 dpi. AUDPC analysis was used to quantify statistical differences between the mutant and PH-1 according to Schandry (2017). The AUDPC values were calculated for each spike infected with PH-1- $\Delta Fgtpp1-1$ or PH-1. Then, AUDPC average values for PH-1- $\Delta Fgtpp1-1$ and PH-1 were calculated, and significant differences between the PH-1- $\Delta Fgtpp1-1$ mutant and PH-1 were calculated using a *t* test with $P < 0.05$.

A bottom-inoculation approach was also performed to assess the virulence of the PH-1- $\Delta Fgtpp1$ mutants and

PH-1- $\Delta Fgtpp1-1::TPP1$ complementation strains compared with wild-type PH-1. This approach is an adaptation of a previously described protocol (Seong et al. 2005). The third and fourth full-sized spikelets from the bottom of the wheat spike were inoculated, one spike per plant, and, typically, 15 plants per fungal strain. Four independent replicates were performed. In each replicate, a similar number of plants was inoculated with each fungal strain (typically 10 to 14), always timed with plant anthesis. The two spikelets at the base were point-inoculated with 5 μl of 5×10^4 conidia/ml of PH-1- $\Delta Fgtpp1-1$, PH-1- $\Delta Fgtpp1-3$, PH-1- $\Delta Fgtpp1-1::TPP1$, or PH-1. Inoculated plants were incubated as described above. Between 10 and 11 dpi and depending upon the disease severity per infection batch, wheat spikes were classified as either completely bleached (wherein all the spikelets were found to be bleached and the awns spread out) or partially bleached (wherein some but not all the spikelets were bleached, and most awns remained upright). A goodness-of-fit test was performed to test if the observed frequencies of fully bleached/partially bleached spikes for each fungal strain were the same or different. The experiment was repeated at least four independent times. Images were captured using Olympus OM-D E-M10 fitted with an M.Zuiko 30-mm F3.5 macro lens.

Fungal detection from infected spikes

Fully beached and partially beached spikes infected with either PH-1- $\Delta Fgtpp1-1$ or wild-type *F. graminearum* PH-1 were harvested at 10 dpi. The rachis from each infected spike was dissected into five segments. The rachis segments were surface sterilized by fully submerging the segments into a solution containing 0.6% bleach and 0.02% Tween 20 for 15 min. The segments were then washed three times with sterile water. The five segments belonging to the same rachis were plated on SNA containing 15 $\mu\text{g}/\text{ml}$ of gentamycin to inhibit bacterial growth. The plates were incubated at room temperature under constant ultraviolet light for 2 days to allow the fungus inside the rachis to grow and spread into the neighboring agar. Images were captured as described above. Three fully bleached and three partially bleached spikes from each fungal strain were assessed, with three uninfected rachises serving as mock controls.

DON mycotoxin measurements

DON mycotoxin concentrations within wheat spikes infected with either the PH-1- $\Delta Fgtpp1$ mutant strains or wild-type *F. graminearum* PH-1 were assessed using the DON Plate Kit (Beacon Analytical Systems). Briefly, the bottom part (8 spikelets from the base and its corresponding rachis segments) of bottom-inoculated wheat spikes infected with either wild-type *F. graminearum* PH-1 or the PH-1- $\Delta Fgtpp1$ were collected at 10 dpi and frozen in liquid nitrogen. Three independent spikes per strain were individually ground to a fine powder. Five volumes of sterile water were added to the ground tissue. Then, the solution was mixed by vortexing and incubated at 30°C for 30 min, and the supernatant was collected after centrifugation at maximum speed (12,000 rpm). The supernatant was 500-fold diluted, and 50 μl of this diluted supernatant was mixed with 50 μl of the enzyme conjugate following the protocol described by the manufacturer. Three independent mock-inoculated wheat spikes were also included as a negative control. A calibration curve using different DON concentrations was used to determine the DON parts per million (ppm) for each wheat spike. The experiment was repeated twice. Each replicate consisted of 12 plants, where three spikes, one spike per plant, were inoculated with the different fungal strains. Mock values were reported as <0.2 ppm, as values were outside the lowest calibrator from the standard curve. An analysis of variance test followed by a Tukey post-hoc test was performed to calculate significant differences

between the $\Delta Fgtp1$ mutants and wild-type *F. graminearum* PH-1 strain ($P < 0.05$).

Generation of plant expression constructs

The RPS5^{D266E}:myc and RbcS-TP:mCherry constructs have been described previously (Helm et al. 2022; Qi et al. 2012).

To generate the FgTPP1:GFP and FgTPP1:mCherry constructs, we used the Golden Gate protocol as previously described by Lampropoulos et al. (2013). Briefly, the *FgTPP1* open reading frame, without the predicted signal peptide and the stop codon, was PCR-amplified using primer combination P30 and P31 using complementary DNA isolated from wheat floral tissue infected with PH-1 as the template. The resulting PCR fragments were purified and combined in a single Golden Gate reaction with the destination vector pGGZ001 for in planta expression. The pGGZ001 plasmid contains a 35S promoter, Ω -element (protein expression enhancer), UBQ10 terminator, HygR resistant cassette, and either mCherry or GFP as C-terminus tags. The resulting constructs were sequence confirmed and subsequently designated as FgTPP1:GFP (pGGZ001-35s- Ω -element-*FgTPP1*:GFP-UBQ10t-HygR) and FgTPP1:mCherry (pGGZ001-35s- Ω -element-*FgTPP1*:mCherry-UBQ10t-HygR). A free GFP construct (pGGZ001-35s- Ω -element-GFP-UBQ10t-HygR) was also generated using the aforementioned Golden Gate protocol.

To generate the FgTPP1:sYFP construct, the *FgTPP1* open reading frame (without the signal peptide sequence) was synthesized by TWIST Biosciences with codon optimization for expression in *N. benthamiana* and cloned into pTWIST-Kan by the service provider. This open reading frame was then PCR-amplified with *attB*-containing primers. The resulting PCR fragments were purified and recombined into the Gateway entry vector, pBSDONR(P1-P4) (Qi et al. 2012), using BP Clonase II (Invitrogen), and the resulting construct was designated pBSDONR(P1-P4):*FgTPP1*. The pBSDONR(P1-P4):*FgTPP1* plasmid was mixed with the pBSDONR(P4r-P2):*sYFP* (Qi et al. 2012) plasmid and the Gateway-compatible expression vector pTA7001 (Vinatzer et al. 2006). Plasmids were recombined by the addition of LR Clonase II (Invitrogen). The resulting construct was designated pTA7001:*FgTPP1*:sYFP. All constructs were sequence-verified for proper sequence and reading frame.

Agrobacterium-mediated transient expression in *N. benthamiana*

Transient protein expression assays were performed as previously described with minor modifications (Helm et al. 2022). Briefly, the constructs described above were mobilized into *Agrobacterium tumefaciens* GV3101 (pMP90) and grown on Luria-Bertani media plates supplemented with 25 μ g/ml of gentamicin sulfate and 50 μ g/ml of kanamycin for 2 days at 30°C. Cultures were prepared in liquid Luria-Bertani media supplemented with the appropriate antibiotics and were shaken overnight at 30°C on an orbital shaker. Following overnight incubation, cells were pelleted by centrifuging at 3,000 rpm for 3 min at room temperature. For confocal microscopy and immunoblot analyses, bacterial pellets were resuspended in 10 mM MgCl₂, adjusted, mixed to an OD₆₀₀ of 0.3 for each strain, and incubated with 100 μ M acetosyringone for 3 to 4 h at room temperature. For the suppression of hypersensitive response-like cell death assay, bacterial pellets of FgTPP1:sYFP and RPS5^{D266E}:myc were resuspended in 10 mM MgCl₂, adjusted to an OD₆₀₀ of 0.3 and 0.15, respectively, and incubated with 150 μ M acetosyringone for 3 h at room temperature. All bacterial suspensions were infiltrated into the abaxial side of *N. benthamiana* leaves using a needleless syringe. For pTA7001-based constructs, which are dexamethasone-inducible, gene expression was induced approx-

imately 48 h post-agroinfiltration by spraying leaves with 50 μ M dexamethasone.

Confocal microscopy

Confocal microscopy of *N. benthamiana* epidermal cells was performed 24 h post-agroinfiltration using a Zeiss LSM880 Axio Examiner upright confocal microscope with a Plan Apochromat 20 \times /0.8 objective. Fluorescence from the GFP-tagged protein fusions was excited using a 488-nm argon laser and detected between 525 and 550 nm. Fluorescence from the mCherry-tagged constructs was excited with a 561-nm helium-neon laser and detected between 565 and 669 nm. All confocal micrographs shown are of single optical sections and processed using the Zeiss Zen Blue Lite program (Carl Zeiss Microscopy).

Immunoblot analyses

N. benthamiana leaves transiently expressing the epitope-tagged constructs were harvested 24 or 48 h following agroinfiltration and flash frozen in liquid nitrogen, and total protein was extracted as previously described by Helm et al. (2022) for immunoblot analyses. Ten microliters of isolated total protein was separated on a 4 to 20% Tris-glycine stain-free polyacrylamide gel (Bio-Rad) at 170 V for 1 h in 1 \times Tris/glycine/SDS running buffer. Total proteins were transferred to nitrocellulose membranes (GE Water and Process Technologies). Membranes were washed with 1 \times Tris-buffered saline (50 mM Tris-HCl, 150 mM NaCl, pH 7.5) solution supplemented with 0.1% Tween 20 (TBST) and blocked in 5% skim milk (wt/vol) (Becton, Dickinson & Company) for at least 1 h at room temperature. Proteins were detected with horseradish peroxidase-conjugated anti-GFP (1:5,000; Miltenyi Biotec) antibodies for 1 h at room temperature. Membranes were washed three times with 1 \times TBST solution and subsequently incubated with Clarity Western ECL (Bio-Rad) substrate solution for 5 min. Imaging of immunoblots was performed with an ImageQuant 500 CCD imaging system.

Chloroplast isolation

Chloroplast isolation was performed as previously described with slight modifications (Petre et al. 2016). *N. benthamiana* leaves transiently expressing the indicated epitope-tagged constructs were harvested 24 h following agroinfiltration, cut into 1 mm² pieces, and incubated in 20 ml of cold isolation buffer (IB) (400 mM sorbitol, 50 mM HEPES KOH 8M, 2 mM EDTA, and 1 mM MgCl₂) for 15 min on ice. Leaf pieces were homogenized with a PT 1200 C Polytron homogenizer (3 \times 5 s full speed), and the lysate was immediately filtered through doubled Miracloth to remove cell debris. The filtrate was collected in 50-ml conical tubes and centrifuged at 3,000 rpm for 10 min at 4°C. The pellet containing the organelles was resuspended in 400 μ l of ice-cold IB, and chloroplasts were isolated by centrifugation on a Percoll gradient (1 ml of 80% vol/vol Percoll/IB and 3 ml of 40% vol/vol Percoll/IB in a 10-ml conical tube) at 4,500 rpm for 10 min at 4°C. Intact chloroplasts were collected from the bottom layer and subsequently used for laser scanning confocal microscopy.

MAPK activity assay

Suppression of chitin-induced MAPK activation in *N. benthamiana* was performed as previously described with slight modifications (Jaiswal et al. 2022). Briefly, *N. benthamiana* leaves transiently expressing either free GFP or GFP-tagged TPP1 (FgTPP1:GFP) were infiltrated with either nuclease-free water (mock treatment) or chitin hexamer dissolved in nuclease-free water (5 μ g/ml; Accurate Chemicals & Scientific Corporation). Leaf discs (10-mm diameter) were harvested and frozen in liquid nitrogen at 0, 5, and 10 min following mock or chitin infiltration. Total protein was extracted as described above.

Proteins were detected using horseradish peroxidase-conjugated anti-GFP (1:5,000; Miltenyi Biotec), anti-plant actin (1:5000; Abbkine), or anti phospho-P42/44 MAPK (1:5000; Cell Signaling Technology), which detects phosphorylated MPK3 and MPK6. Membranes were washed three times with 1× TBST solution and subsequently incubated with Clarity Western ECL (Bio-Rad) substrate solution for 5 min. Imaging of immunoblots was performed with an ImageQuant 500 CCD imaging system. Experiments were performed at least three independent times with similar results.

Luminol-based ROS assay in *N. benthamiana*

Suppression of ROS production in *N. benthamiana* was performed as previously described using a luminol-based chemiluminescence assay (Jaiswal et al. 2022; Rogers et al. 2024). *N. benthamiana* leaf discs (5-mm diameter) transiently expressing either free GFP or FgTPP1:GFP were harvested 2 days post-agroinfiltration using a cork borer, gently washed three times in nuclease-free water, and incubated overnight in sterile water in a 96-well OptiPlate microplate (Perkin Elmer). The following day, the deionized water was replaced with chitin elicitation solution (luminol [30 µg/ml], horseradish peroxidase [20 µg/ml], chitin hexamer [5 µg/ml] [Accurate Chemicals & Scientific Corporation], and nuclease-free water), and ROS production was monitored by chemiluminescence for 40 min in a microplate reader (Tecan Infinite M200 Pro). Experiments were performed at least three independent times with similar results.

Cell death suppression assay

Forty-eight hours following agroinfiltration with either empty vector, FgTPP1:sYFP, or RPS5^{D266E}:myc, *N. benthamiana* leaves were sprayed with 50 µM dexamethasone supplemented with 0.02% Tween 20 (to induce expression of both RPS5^{D266E}:myc and FgTPP1:sYFP). At 16 h post-transgene induction, *N. benthamiana* leaves were assessed for cell death and photographed under white and ultraviolet light. Experiments were performed at least three independent times with similar results.

TPP1 sequence analysis from *F. graminearum* global populations, dN/dS analysis, and phylogenetic analyses

Haplotype analysis of *FgTPP1* nucleotide sequences from *F. graminearum* isolates was conducted according to Darma et al. (2024). Briefly, *FgTPP1* nucleotide sequences from *F. graminearum* isolates available in the NCBI database were extracted using BLAST+ v2.9.0+ (Camacho et al. 2009) and parsed into a FASTA file using ‘BLASTtoGFF_multiple.py’ (DOI:10.5281/zenodo.13651118). *FgTPP1* coding sequences from 28 *F. graminearum* isolates tested in this study are listed in the Supplementary File S1. *FgTPP1* sequences were aligned using Geneious 10.2.3 alignment with the Blosom62 cost matrix. Introns from those sequences were trimmed to generate coding sequences of *FgTPP1* from global populations. Allele networks from *FgTPP1* coding sequences were generated with POPART v1.7 (Leigh and Bryant 2015) using the minimum spanning network setting.

Pairwise dN/dS ratios were calculated using MEGA11 (Tamura et al. 2021) to assess selection pressure on the *FgTPP1* gene. The Tamura-Nei model (Tamura and Nei 1993) was applied to account for transition/transversion bias, and dN/dS ratios were estimated with standard errors calculated via 1,000 bootstrap replicates. A ratio <1 was interpreted as purifying selection, whereas >1 indicated positive selection.

TPP1 protein sequences from *Fusarium* spp. and other fungi were extracted with BlastP. Multiple hits representing TPP1 homologs from different *Fusarium* species complexes were selected for further analysis. In addition, hits from other fungi,

excluding *Fusarium* species, predicted as trypsin or serine protease with the minimum max score 243, were extracted for further analysis. TPP1 protein sequences from *Fusarium* species and other fungi were aligned using Geneious 10.2.3 alignment as described previously. An amino acid alignment of TPP1 proteins from *Fusarium* spp. and other fungi is available in Supplementary File S2. IQ-Tree 2.2.2.6 (Kalyaanamoorthy et al. 2017; Nguyen et al. 2015) was used to identify the best amino acid substitution model from the TPP1 amino acid sequence alignment and was used to generate a maximum likelihood tree using 10,000 bootstrap replicates. In addition, a Bayesian inference tree was generated to support the maximum likelihood tree using MrBayes 3.2.6 (Huelsenbeck and Ronquist 2001) with the following settings: rate matrix (fixed) WAG, rate variation gamma, gamma categories 4, chain length 1,000,000, heated chains 4, heated chain temperature 0.2, subsampling frequency 10,000, burn-in length 100,000, and random seed 16,291. Finally, Figtree 1.4.4 (Rambaut 2018) was used to refine the appearance of the phylogenetic tree.

Acknowledgments

We thank Tesfaye Mengiste (Purdue University) for access to the microplate reader for the ROS suppression assays, Terri Cameron for technical assistance, the Purdue University Imaging Facility for access to the Zeiss LSM880 Axio Examiner upright confocal microscope, Fiona Dooohan (University of Dublin, Ireland) for providing the pGAD-*SUC2*²²⁻⁵¹¹ plasmid and the *suc2* yeast mutant, Silvia Melina Velasquez for her technical assistance with the violin plots, and Fiona Gilzean and the facilities team at Rothamsted Research for preparing and maintaining the various growth rooms used in this study while major refurbishment of the containment facilities were in progress. All experiments involving *F. graminearum* strain PH-1 and isogenic transformants were conducted in biological containment facilities under U.K. Defra license number 101948/198285.

Literature Cited

- Ade, J., DeYoung, B. J., Golstein, C., and Innes, R. W. 2007. Indirect activation of a plant nucleotide binding site–leucine-rich repeat protein by a bacterial protease. *Proc. Natl. Acad. Sci. U.S.A.* 104:2531–2536.
- Armer, V. J., Kroll, E., Darino, M., Smith, D. P., Urban, M., and Hammond-Kosack, K. E. 2024a. Navigating the *Fusarium* species complex: Host-range plasticity and genome variations. *Fungal Biol.* 128: 2439–2459.
- Armer, V. J., Urban, M., Ashfield, T., Deeks, M. J., and Hammond-Kosack, K. E. 2024b. The trichothecene mycotoxin deoxynivalenol facilitates cell-to-cell invasion during wheat-tissue colonization by *Fusarium graminearum*. *Mol. Plant Pathol.* 25:e13485.
- Bai, G., and Shaner, G. 2004. Management and resistance in wheat and barley to *Fusarium* head blight. *Annu. Rev. Phytopathol.* 42:135–161.
- Bentham, A. R., De la Concepcion, J. C., Mukhi, N., Zdrzalek, R., Draeger, M., Gorenkin, D., Hughes, R. K., and Banfield, M. J. 2020. A molecular roadmap to the plant immune system. *J. Biol. Chem.* 295:14916–14935.
- Brown, N. A., Antoniwi, J., and Hammond-Kosack, K. E. 2012. The predicted secretome of the plant pathogenic fungus *Fusarium graminearum*: A refined comparative analysis. *PLoS One* 7:e33731.
- Brown, N. A., Bass, C., Baldwin, T. K., Chen, H., Massot, F., Carion, P. W. C., Urban, M., van de Meene, A. M. L., and Hammond-Kosack, K. E. 2011. Characterisation of the *Fusarium graminearum*-wheat floral interaction. *J. Pathog.* 2011:626345.
- Brown, N. A., Evans, J., Mead, A., and Hammond-Kosack, K. E. 2017. A spatial temporal analysis of the *Fusarium graminearum* transcriptome during symptomless and symptomatic wheat infection. *Mol. Plant Pathol.* 18:1295–1312.
- Camacho, C., Coulouris, G., Avagyan, V., Ma, N., Papadopoulos, J., Bealer, K., and Madden, T. L. 2009. BLAST+: Architecture and applications. *BMC Bioinform.* 10:421.
- Carter, M. E., Helm, M., Chapman, A. V. E., Wan, E., Restrepo Sierra, A. M., Innes, R. W., Bogdanove, A. J., and Wise, R. P. 2019. Convergent evolution of effector protease recognition by *Arabidopsis* and barley. *Mol. Plant-Microbe Interact.* 32:550–565.
- Catlett, N. L., Lee, B.-N., Yoder, O. C., and Turgeon, B. G. 2003. Split-marker recombination for efficient targeted deletion of fungal genes. *Fungal Genet. Rep.* 50:9–11.

- Cavinder, B., Sikhakolli, U., Fellows, K. M., and Trail, F. 2012. Sexual development and ascospore discharge in *Fusarium graminearum*. *J. Vis. Exp.* 2012:e3895.
- Chandrasekaran, M., Thangavelu, B., Chun, S. C., and Sathiyabama, M. 2016. Proteases from phytopathogenic fungi and their importance in phytopathogenicity. *J. Gen. Plant Pathol.* 82:233-239.
- Chen, J., Zhang, X., Rathjen, J. P., and Dodds, P. N. 2022. Direct recognition of pathogen effectors by plant NLR immune receptors and downstream signalling. *Essays Biochem.* 66:471-483.
- Cuomo, C. A., Güldener, U., Xu, J.-R., Trail, F., Turgeon, B. G., Di Pietro, A., Walton, J. D., Ma, L.-J., Baker, S. E., Rep, M., Adam, G., Antoniw, J., Baldwin, T., Calvo, S., Chang, Y.-L., Decaprio, D., Gale, L. R., Gnerre, S., Goswami, R. S., Hammond-Kosack, K., Harris, L. J., Hilburn, K., Kennell, J. C., Kroken, S., Magnuson, J. K., Mannhaupt, G., Mauceli, E., Mewes, H.-W., Mitterbauer, R., Muehlbauer, G., Münsterkötter, M., Nelson, D., O'Donnell, K., Ouellet, T., Qi, W., Quesneville, H., Roncero, M. I. G., Seong, K.-Y., Tetko, I. V., Urban, M., Waalwijk, C., Ward, T. J., Yao, J., Birren, B. W., and Kistler, H. C. 2007. The *Fusarium graminearum* genome reveals a link between localized polymorphism and pathogen specialization. *Science* 317:1400-1402.
- Cuzick, A., Urban, M., and Hammond-Kosack, K. 2008. *Fusarium graminearum* gene deletion mutants *map1* and *tri5* reveal similarities and differences in the pathogenicity requirements to cause disease on Arabidopsis and wheat floral tissue. *New Phytol.* 177:990-1000.
- Darino, M., Urban, M., Kaur, N., Wood, A. M., Grimwade-Mann, M., Smith, D., Beacham, A., and Hammond-Kosack, K. 2024. Identification and functional characterisation of a locus for target site integration in *Fusarium graminearum*. *Fungal Biol. Biotechnol.* 11:2.
- Darma, R., Yu, D. S., Outram, M. A., Sung, Y.-C., Hill, E. H., Croll, D., Williams, S. J., Ovenden, B., Milgate, A., Solomon, P. S., and McDonald, M. C. 2024. Revisiting the evolution and function of NIP2 paralogs in the *Rhynchosporium* spp. complex. *bioRxiv*. <https://doi.org/10.1101/2024.10.15.618441>
- Dean, R., van Kan, J. A. L., Pretorius, Z. A., Hammond-Kosack, K. E., Di Pietro, A., Spanu, P. D., Rudd, J. J., Dickman, M., Kahmann, R., Ellis, J., and Foster, G. D. 2012. The top 10 fungal pathogens in molecular plant pathology. *Mol. Plant Pathol.* 13:414-430.
- Deng, C., Leonard, A., Cahill, J., Lv, M., Li, Y., Thatcher, S., Li, X., Zhao, X., Du, W., Li, Z., Li, H., Llaca, V., Fengler, K., Marshall, L., Harris, C., Tabor, G., Li, Z., Tian, Z., Yang, Q., Chen, Y., Tang, J., Wang, X., Hao, J., Yan, J., Lai, Z., Fei, X., Song, W., Lai, J., Zhang, X., Shu, G., Wang, Y., Chang, Y., Zhu, W., Xiong, W., Sun, J., Li, B., and Ding, J. 2022. The RppC-AvrRppC NLR-effector interaction mediates the resistance to southern corn rust in maize. *Mol. Plant* 15:904-912.
- Ding, P., and Ding, Y. 2020. Stories of salicylic acid: A plant defense hormone. *Trends Plant Sci.* 25:549-565.
- Engler, C., Gruetzer, R., Kandzia, R., and Marillonnet, S. 2009. Golden gate shuffling: A one-pot DNA shuffling method based on type IIs restriction enzymes. *PLoS One* 4:e5553.
- Figueroa, M., Hammond-Kosack, K. E., and Solomon, P. S. 2018. A review of wheat diseases—A field perspective. *Mol. Plant Pathol.* 19: 1523-1536.
- Figueroa, M., Ortiz, D., and Henningsen, E. C. 2021. Tactics of host manipulation by intracellular effectors from plant pathogenic fungi. *Curr. Opin. Plant Biol.* 62:102054.
- Galvez-Valdivieso, G., and Mullineaux, P. M. 2010. The role of reactive oxygen species in signaling from chloroplasts to the nucleus. *Physiol. Planta* 138:430-439.
- Hao, G., McCormick, S., Usgaard, T., Tiley, H., and Vaughan, M. M. 2020. Characterization of three *Fusarium graminearum* effectors and their roles during *Fusarium* head blight. *Front. Plant Sci.* 11:579553.
- Hao, G., McCormick, S., Vaughan, M. M., Naumann, T. A., Kim, H.-S., Proctor, R., Kelly, A., and Ward, T. J. 2019. *Fusarium graminearum* arabinanase (Arb93B) enhances wheat head blight susceptibility by suppressing plant immunity. *Mol. Plant-Microbe Interact.* 32: 888-898.
- Hao, G., Naumann, T. A., Chen, H., Bai, G., McCormick, S., Kim, H.-S., Tian, B., Trick, H. N., Naldrett, M. J., and Proctor, R. 2023. *Fusarium graminearum* effector FgNls1 targets plant nuclei to induce wheat head blight. *Mol. Plant-Microbe Interact.* 36:478-488.
- Helm, M., Qi, M., Sarkar, S., Yu, H., Whitham, S. A., and Innes, R. W. 2019. Engineering a decoy substrate in soybean to enable recognition of the soybean mosaic virus N1a protease. *Mol. Plant-Microbe Interact.* 32:760-769.
- Helm, M., Singh, R., Hiles, R., Jaiswal, N., Myers, A., Iyer-Pascuzzi, A. S., and Goodwin, S. B. 2022. Candidate effector proteins from the maize tar spot pathogen *Phyllachora maydis* localize to diverse plant cell compartments. *Phytopathology* 112:2538-2548.
- Hohn, T. M., and Desjardins, A. E. 1992. Isolation and gene disruption of the *Tox5* gene encoding trichodiene synthase in *Gibberella pulicaris*. *Mol. Plant-Microbe Interact.* 5:249-256.
- Huelsenbeck, J. P., and Ronquist, F. 2001. MRBAYES: Bayesian inference of phylogenetic trees. *Bioinformatics* 17:754-755.
- Jaiswal, N., Liao, C.-J., Mengesha, B., Han, H., Lee, S., Sharon, A., Zhou, Y., and Mengiste, T. 2022. Regulation of plant immunity and growth by tomato receptor-like cytoplasmic kinase TRK1. *New Phytol.* 233:458-478.
- Jaiswal, N., Myers, A., Weese, T. L., Carter, M. E., Scofield, S. R., and Helm, M. 2023. Analysis of cell death induction by the barley NLR immune receptor PBR1. *PhytoFrontiers* 3:663-678.
- Jashni, M. K., Mehrabi, R., Collemare, J., Mesarich, C. H., and de Wit, P. J. G. M. 2015. The battle in the apoplast: Further insights into the roles of proteases and their inhibitors in plant-pathogen interactions. *Front. Plant Sci.* 6:584.
- Jiang, C., Hei, R., Yang, Y., Zhang, S., Wang, Q., Wang, W., Zhang, Q., Yan, M., Zhu, G., Huang, P., Liu, H., and Xu, J.-R. 2020. An orphan protein of *Fusarium graminearum* modulates host immunity by mediating proteasomal degradation of TaSnRK1 α . *Nat. Commun.* 11:4382.
- Johns, L. E., Bebb, D. P., Gurr, S. J., and Brown, N. A. 2022. Emerging health threat and cost of *Fusarium* mycotoxins in European wheat. *Nat. Food* 3:1014-1019.
- Kalyaanamoorthy, S., Minh, B. Q., Wong, T. K. F., von Haeseler, A., and Jermini, L. S. 2017. ModelFinder: Fast model selection for accurate phylogenetic estimates. *Nat. Methods* 14:587-589.
- Kanja, C., Machado-Wood, A. K., Baggaley, L., Walker, C., and Hammond-Kosack, K. E. 2021. Cereal-*Fusarium* interactions: Improved fundamental insights into *Fusarium* pathogenomics and cereal host resistance reveals new ways to achieve durable disease control. In: *Achieving Durable Disease Resistance in Cereals*. R. Oliver, ed. Burleigh Dodds Science Publishing, Sawston, Cambridge, United Kingdom.
- Kim, M. G., da Cunha, L., McFall, A. J., Belkadir, Y., DebRoy, S., Dangl, J. L., and Mackey, D. 2005. Two *Pseudomonas syringae* type III effectors inhibit RIN4-regulated basal defense in *Arabidopsis*. *Cell* 121: 749-759.
- Kim, S. H., Qi, D., Ashfield, T., Helm, M., and Innes, R. W. 2016. Using decoys to expand the recognition specificity of a plant disease resistance protein. *Science* 351:684-687.
- King, R., Urban, M., and Hammond-Kosack, K. E. 2017a. Annotation of *Fusarium graminearum* (PH-1) version 5.0. *Genome Announc.* 5:e01479-16.
- King, R., Urban, M., Hammond-Kosack, M. C. U., Hassani-Pak, K., and Hammond-Kosack, K. E. 2015. The completed genome sequence of the pathogenic ascomycete fungus *Fusarium graminearum*. *BMC Genomics* 16:544.
- King, R., Urban, M., Lauder, R. P., Hawkins, N., Evans, M., Plummer, A., Halsey, K., Lovegrove, A., Hammond-Kosack, K., and Rudd, J. J. 2017b. A conserved fungal glycosyltransferase facilitates pathogenesis of plants by enabling hyphal growth on solid surfaces. *PLoS Pathog.* 13: e1006672.
- Kretschmer, M., Damoo, D., Djamei, A., and Kronstad, J. 2020. Chloroplasts and plant immunity: Where are the fungal effectors? *Pathogens* 9:19.
- Kroll, E., Bayon, C., Rudd, J., Armer, V. J., Magaji-Umashankar, A., Ames, R., Urban, M., Brown, N. A., and Hammond-Kosack, K. 2025. A conserved fungal Knr4/Smi1 protein is crucial for maintaining cell wall stress tolerance and host plant pathogenesis. *PLoS Pathog.* 21:e1012769.
- Lampropoulos, A., Sutikovic, Z., Wenzl, C., Maegele, I., Lohmann, J. U., and Forner, J. 2013. GreenGate - a novel, versatile, and efficient cloning system for plant transgenesis. *PLoS One* 8:e83043.
- Leigh, J. W., and Bryant, D. 2015. POPART: Full-feature software for haplotype network construction. *Methods Ecol. Evol.* 6:1110-1116.
- Littlejohn, G. R., Breen, S., Smirnoff, N., and Grant, M. 2021. Chloroplast immunity illuminated. *New Phytol.* 229:3088-3107.
- Liu, J., Gong, P., Lu, R., Lozano-Durán, R., Zhou, X., and Li, F. 2024. Chloroplast immunity: A cornerstone of plant defense. *Mol. Plant* 17:686-688.
- Liu, K., Wang, X., Qi, Y., Li, Y., Shi, Y., Ren, Y., Wang, A., Cheng, P., and Wang, B. 2024. Effector protein serine carboxypeptidase FgSCP is essential for full virulence in *Fusarium graminearum* and is involved in modulating plant immune responses. *Phytopathology* 114:2131-2142.
- Lu, S., and Edwards, M. C. 2016. Genome-wide analysis of small secreted cysteine-rich proteins identifies candidate effector proteins potentially involved in *Fusarium graminearum*-wheat interactions. *Phytopathology* 106:166-176.
- McCombe, C. L., Greenwood, J. R., Solomon, P. S., and Williams, S. J. 2022. Molecular plant immunity against biotrophic, hemibiotrophic, and necrotrophic fungi. *Essays Biochem.* 66:581-593.

- Meng, E. C., Goddard, T. D., Pettersen, E. F., Couch, G. S., Pearson, Z. J., Morris, J. H., and Ferrin, T. E. 2023. UCSF ChimeraX: Tools for structure building and analysis. *Protein Sci.* 32:e4792.
- Menke, J. R. 2011. A study of *Fusarium graminearum* virulence factors. Ph.D. dissertation. University of Minnesota, St. Paul, MN. <https://hdl.handle.net/11299/119322>
- Mentges, M., Glasenapp, A., Boenisch, M., Malz, S., Henrissat, B., Frandsen, R. J. N., Güldener, U., Münsterkötter, M., Bormann, J., Lebrun, M.-H., Schäfer, W., and Martínez-Rocha, A. L. 2020. Infection cushions of *Fusarium graminearum* are fungal arsenals for wheat infection. *Mol. Plant Pathol.* 21:1070-1087.
- Miltenburg, M. G., Bonner, C., Hepworth, S., Huang, M., Rampitsch, C., and Subramaniam, R. 2022. Proximity-dependent biotinylation identified a suite of candidate effector proteins from *Fusarium graminearum*. *Plant J.* 112:369-382.
- Mirdita, M., Schütze, K., Moriwaki, Y., Heo, L., Ovchinnikov, S., and Steinegger, M. 2022. ColabFold: Making protein folding accessible to all. *Nat. Methods* 19:679-682.
- Nelson, B. K., Cai, X., and Nebenführ, A. 2007. A multicolored set of *in vivo* organelle markers for co-localization studies in Arabidopsis and other plants. *Plant J.* 51:1126-1136.
- Nganje, W. E., Kaitibie, S., Wilson, W. W., Leistritz, F. L., and Bangsund, D. A. 2004. Economic impacts of Fusarium head blight in wheat and barley: 1993-2001. *Agribusiness and Applied Economics Report No. 538*. Agricultural Experiment Station, North Dakota State University, Fargo, ND.
- Ngou, B. P. M., Ding, P., and Jones, J. D. G. 2022. Thirty years of resistance: Zig-zag through the plant immune system. *Plant Cell* 34:1447-1478.
- Nguyen, L.-T., Schmidt, H. A., von Haeseler, A., and Minh, B. Q. 2015. IQ-TREE: A fast and effective stochastic algorithm for estimating maximum-likelihood phylogenies. *Mol. Biol. Evol.* 32:268-274.
- Petre, B., Lorrain, C., Saunders, D. G. O., Win, J., Sklenar, J., Duplessis, S., and Kamoun, S. 2016. Rust fungal effectors mimic host transit peptides to translocate into chloroplasts. *Cell. Microbiol.* 18:453-465.
- Petre, B., Saunders, D. G. O., Sklenar, J., Lorrain, C., Win, J., Duplessis, S., and Kamoun, S. 2015. Candidate effector proteins of the rust pathogen *Melampsora larici-populina* target diverse plant cell compartments. *Mol. Plant-Microbe Interact.* 28:689-700.
- Pottinger, S. E., Bak, A., Margets, A., Helm, M., Tang, L., Casteel, C., and Innes, R. W. 2020. Optimizing the PBS1 decoy system to confer resistance to Potyvirus infection in *Arabidopsis* and soybean. *Mol. Plant-Microbe Interact.* 33:932-944.
- Qi, D., DeYoung, B. J., and Innes, R. W. 2012. Structure-function analysis of the coiled-coil and leucine-rich repeat domains of the RPS5 disease resistance protein. *Plant Physiol.* 158:1819-1832.
- Qiu, H., Zhao, X., Fang, W., Wu, H., Abubakar, Y. S., Lu, G.-d., Wang, Z., and Zheng, W. 2019. Spatiotemporal nature of *Fusarium graminearum*-wheat coleoptile interactions. *Phytopathol. Res.* 1:26.
- Rambaut, A. 2018. FigTree v1.4.4: Molecular Evolution, Phylogenetics and Epidemiology. University of Edinburgh, Edinburgh, United Kingdom.
- Redditt, T. J., Chung, E.-H., Karimi, H. Z., Rodibaugh, N., Zhang, Y., Trinidad, J. C., Kim, J. H., Zhou, Q., Shen, M., Dangel, J. L., Mackey, D., and Innes, R. W. 2019. AvrRpm1 functions as an ADP-ribosyl transferase to modify NOI domain-containing proteins, including Arabidopsis and soybean RPM1-Interacting Protein4. *Plant Cell* 31:2664-2681.
- Rhodes, J., Zipfel, C., Jones, J. D. G., and Ngou, B. P. M. 2022. Concerted actions of PRR- and NLR-mediated immunity. *Essays Biochem.* 66:501-511.
- Rogers, A., Jaiswal, N., Roggenkamp, E., Kim, H.-S., MacCready, J. S., Chilvers, M. I., Scofield, S. R., Iyer-Pascuzzi, A. S., and Helm, M. 2024. Genome-informed trophic classification and functional characterization of virulence proteins from the maize tar spot pathogen *Phyllachora maydis*. *Phytopathology* 114:1940-1949.
- Rudd, J. J., Antoniw, J., Marshall, R., Motteram, J., Fraaije, B., and Hammond-Kosack, K. 2010. Identification and characterisation of *Mycosphaerella graminicola* secreted or surface-associated proteins with variable intragenic coding repeats. *Fungal Genet. Biol.* 47:19-32.
- Schandry, N. 2017. A practical guide to visualization and statistical analysis of *R. solanacearum* infection data using R. *Front. Plant Sci.* 8:623.
- Selin, C., de Kievit, T. R., Belmonte, M. F., and Fernando, W. G. D. 2016. Elucidating the role of effectors in plant-fungal interactions: Progress and challenges. *Front. Microbiol.* 7:600.
- Seong, K., Hou, Z., Tracy, M., Kistler, H. C., and Xu, J.-R. 2005. Random insertional mutagenesis identifies genes associated with virulence in the wheat scab fungus *Fusarium graminearum*. *Phytopathology* 95:744-750.
- Shao, F., Golstein, C., Ade, J., Stoutemyer, M., Dixon, J. E., and Innes, R. W. 2003. Cleavage of *Arabidopsis* PBS1 by a bacterial type III effector. *Science* 301:1230-1233.
- Simonich, M. T., and Innes, R. W. 1995. A disease resistance gene in *Arabidopsis* with specificity for the *avrPph3* gene of *Pseudomonas syringae* pv. *phaseolicola*. *Mol. Plant-Microbe Interact.* 8:637-640.
- Simons, G., Groenendijk, J., Wijbrandi, J., Reijans, M., Groenen, J., Diergaarde, P., Van der Lee, T., Bleeker, M., Onstenk, J., de Both, M., Haring, M., Mes, J., Cornelissen, B., Zabeau, M., and Vos, P. 1998. Dissection of the *Fusarium I2* gene cluster in tomato reveals six homologs and one active gene copy. *Plant Cell* 10:1055-1068.
- Sperschneider, J., Catanzariti, A.-M., DeBoer, K., Petre, B., Gardiner, D. M., Singh, K. B., Dodds, P. N., and Taylor, J. M. 2017. LOCALIZER: Sub-cellular localization prediction of both plant and effector proteins in the plant cell. *Sci. Rep.* 7:44598.
- Tamura, K., and Nei, M. 1993. Estimation of the number of nucleotide substitutions in the control region of mitochondrial DNA in humans and chimpanzees. *Mol. Biol. Evol.* 10:512-526.
- Tamura, K., Stecher, G., and Kumar, S. 2021. MEGA 11: Molecular Evolutionary Genetics Analysis Version 11. *Mol. Biol. Evol.* 38:3022-3027.
- Teufel, F., Almagro Armenteros, J. J., Johansen, A. R., Gislason, M. H., Pihl, S. I., Tsirigos, K. D., Winther, O., Brunak, S., von Heijne, G., and Nielsen, H. 2022. SignalP 6.0 predicts all five types of signal peptides using protein language models. *Nat. Biotechnol.* 40:1023-1025.
- Urban, M., Mott, E., Farley, T., and Hammond-Kosack, K. 2003. The *Fusarium graminearum* MAP1 gene is essential for pathogenicity and development of perithecia. *Mol. Plant Pathol.* 4:347-359.
- Vinatzer, B. A., Teitzel, G. M., Lee, M.-W., Jelenska, J., Hotton, S., Fairfax, K., Jenrette, J., and Greenberg, J. T. 2006. The type III effector repertoire of *Pseudomonas syringae* pv. *syringae* B728a and its role in survival and disease on host and non-host plants. *Mol. Microbiol.* 62:26-44.
- Waalwijk, C., Taga, M., Zheng, S.-L., Proctor, R. H., Vaughan, M. M., and O'Donnell, K. 2018. Karyotype evolution in *Fusarium*. *IMA Fungus* 9:13-26.
- Wang, C., Zheng, Y., Liu, Z., Qian, Y., Li, Y., Yang, L., Liu, S., Liang, W., and Li, J. 2023. The secreted FolAsp aspartic protease facilitates the virulence of *Fusarium oxysporum* f. sp. *lycopersici*. *Front. Microbiol.* 14:1103418.
- Wang, X., He, M., Liu, H., Ding, H., Liu, K., Li, Y., Cheng, P., Li, Q., and Wang, B. 2022. Functional characterization of the M36 metalloprotease FgFly1 in *Fusarium graminearum*. *J. Fungi* 8:726.
- Wood, A. K. M., Walker, C., Lee, W.-S., Urban, M., and Hammond-Kosack, K. E. 2020. Functional evaluation of a homologue of plant rapid alkalisation factor (RALF) peptides in *Fusarium graminearum*. *Fungal Biol.* 124:753-765.
- Xiong, J., Luo, M., Chen, Y., Hu, Q., Fang, Y., Sun, T., Hu, G., and Zhang, C.-J. 2024. Subtilisin-like proteases from *Fusarium graminearum* induce plant cell death and contribute to virulence. *Plant Physiol.* 195:1681-1693.
- Xu, L., Wang, H., Zhang, C., Wang, J., Chen, A., Chen, Y., and Ma, Z. 2020. System-wide characterization of subtilases reveals that subtilisin-like protease FgPrb1 of *Fusarium graminearum* regulates fungal development and virulence. *Fungal Genet. Biol.* 144:103449.
- Xu, Q., Tang, C., Wang, X., Sun, S., Zhao, J., Kang, Z., and Wang, X. 2019. An effector protein of the wheat stripe rust fungus targets chloroplasts and suppresses chloroplast function. *Nat. Commun.* 10:5571.
- Zhang, J., Li, W., Xiang, T., Liu, Z., Laluk, K., Ding, X., Zou, Y., Gao, M., Zhang, X., Chen, S., Mengiste, T., Zhang, Y., and Zhou, J.-M. 2010. Receptor-like cytoplasmic kinases integrate signaling from multiple plant immune receptors and are targeted by a *Pseudomonas syringae* effector. *Cell Host Microbe* 7:290-301.
- Zhou, B., Benbow, H. R., Brennan, C. J., Arunachalam, C., Karki, S. J., Mullins, E., Feechan, A., Burke, J. I., and Doohan, F. M. 2020. Wheat encodes small, secreted proteins that contribute to resistance to Septoria tritici blotch. *Front. Genet.* 11:469.